Synthesis, Structural and Physical Properties of $Ba_xNi_{1-x}Fe_2O_4$ ($0 \leq x \geq 1$) Nanomaterials

Qurat ul Ain Arif Paracha

Regn. No.00000172975

This work is submitted as a MS thesis in partial fulfillment of the requirement for the degree of Master of Science

In

Chemistry

Supervised by: Dr.Zahida Malik

Department of Chemistry

School of Natural Sciences (SNS)

National University of Sciences & Technology (NUST)

Islamabad, Pakistan

2018

FORM TH-4

National University of Sciences & Technology

MS THESIS WORK

We hereby recommend that the dissertation prepared under our supervision by: QURAT UL AIN ARIF PARACHA, Regn No. 00000172975 Titled: Synthesis, Structural and Physical Properties of $Ba_x Ni_{1-x} Fe_2O_4$ ($0 \leq x \geq 1$) Nanomaterials be accepted in partial fulfillment of the requirements for the award of **MS** degree.

Examination Committee Members

1. Name: DR. AZHAR MAHMOOD Signature: _____

2. Name: DR. FOUZIA PARVEEN MALIK Signature: _____

3. Name: DR. RAHAN ZAFAR PARACHA Signature: _____

External Examiner: DR. NASIR MAHBOOB Signature: _____

Supervisor's Name: DR. ZAHIDA MALIK Signature: _____

Co-Supervisor's Name: DR. NASEEM IQBAL Signature: _____

_____ 13/08/18
Head of Department Date

COUNTERSINGED

Date: 13/08/18 _____
Dean/Principal

THESIS ACCEPTANCE CERTIFICATE

Certified that final copy of MS thesis written by **Ms. Qurat ul Ain Arif Paracha**, (Registration No. **00000172975**), of **School of Natural Sciences** has been vetted by undersigned, found complete in all respects as per NUST statutes/regulations, is free of plagiarism, errors, and mistakes and is accepted as partial fulfillment for award of MS/M.Phil degree. It is further certified that necessary amendments as pointed out by GEC members and external examiner of the scholar have also been incorporated in the said thesis.

Signature: _____

Name of Supervisor: Dr. Zahida Malik

Date: 13/08/18

Signature (HoD): _____

Date: 13/08/18

Signature (Dean/Principal): _____

Date: 13/08/18

Dedicated To

My Parents

Acknowledgements

IN THE NAME OF ALLAH, THE MOST GRACIOUS AND THE MOST MERCIFUL'
"SURELY, ALLAH IS WITH THOSE WHO ARE AS-SAABIROON (THE PATIENT)" [AL QURAN 6:46]

First, giving all honors to Almighty Allah from whom all blessings fall, and without whom I am nothing and may the peace and blessings be on the most noble of Prophets and Messengers, our Prophet Muhammad (P.B.U.H)

I would like to express my deepest gratitude to my supervisor Dr. Zahida Malik from SNS, NUST for her guidance, cooperation and invaluable advice. Her constructive comments and suggestions throughout the experimental and thesis work have contributed to the success of this research. Her timely and efficient contributions helped me to shape this thesis in its final form. I consider it my privilege to have accomplished this thesis under her right guidance.

I would like to express my warmest thanks to my Co-supervisor Dr.Naseem Iqbal as he has helped me greatly during my research work and has always been extremely supportive and nice to me. I am very thankful to Dr. Fouzia Malik, Dr. Rehan Zafar Paracha, Dr. Azhar Mahmood and Dr. Rizwan Nasir Paracha for their valuable guidance and scholarly inputs. I would like to mention the name of Dr. Nasir Mehboob from Ripah International University, Islamabad who persisted a great guide and support during my work.

I owe a deep sense of gratitude to my friends Naila Jabbar, Aneeqa Safdar, Effat Sitara and Muhammad Adeel for their constant moral support and encouragement. Finally, an honorable mention goes to my family members. I am forever indebted to my mother and father for their unconditional love and endless duas. I would like to extend my deepest gratitude to my siblings Dr.Faiza, Aezaz Raheem, Dr Awais and my brother in law Khurram Hameed for their prayer and moral support.

Qurat ul Ain Arif Paracha

Abstract

Now a days, research on nickel ferrite nanoparticles is dominated owing to their distinguished structural and physical properties resulting large scale applications in almost every field of life. This research work presents synthesis, characterization and determination of dielectric, magnetic and optical properties of barium doped nickel ferrite nanoparticles i.e. $Ba_xNi_{1-x}Fe_2O_4$ ($0 \leq x \geq 1$). These nanoparticles were successfully synthesized via hydrothermal method by applying suitable reaction conditions. XRD, SEM and EDX were used to characterize prepared nanoparticles. XRD analysis revealed that barium doped samples have cubic spinel structure and their crystallite size decreases from 72.6-42.8 nm by barium addition. SEM micrographs shows that prepared nanoparticles have spherical in shape and upon doping increase in particle size have been observed. In order to determine elemental composition EDX was employed that confirms the purity of samples as there is no impurity peak is present in EDX spectra. Band gap ranging from 2.1-5.5ev has obtained from Tauc plot. Dielectric properties like values of Dielectric constant, Dielectric loss, tan loss and AC conductivity was estimated and it is interesting to note that sample having maximum concentration of Barium have highest value of dielectric loss and dielectric constant i.e 8.3×10^4 and 2.7×10^4 Fm^{-1} respectively. So, it can be best candidate for charge storing applications while for AC conductivity and tan loss no periodic trend was observed but all samples show common behavior that they have large values of AC conductivity at higher frequency. Magnetic Properties was determined by Fluxgate DC magnetometer and it divulges that there is decrease in values of saturation magnetization while increase in coercivity values with doping.

Table of Contents

List of Figures

List of tables

Abbreviations

SEM	Scanning Electron Microscopy
UV	Ultra Violet
VIS	Visible
XRPD	X-Ray Powder Diffraction
TEM	Tunneling Electron Microscope
DRS	Diffuse Reflectance Spectroscopy
LCR	Resistor, Capacitor and Inductor
XRPD	X-Ray Powder Diffraction
EDX	Energy Dispersive X-Ray Spectroscopy
TEM	Transmission Electron Microscope
DUT	Device under Test
FWHM	Full Width Half Maxima
ev	Electron Volt
VSM	Vibrating sample Magnetometer

CHAPTER 1

Introduction

1.1. Nanotechnology.

The word "Nano" has been coined from the Greek word "Nanos" meaning 'dwarf'. It is one billionth part of a meter (10^{-9} m). So, Nanoscience and is the branch of science which deals with the study of materials having at least size of one dimension is in the range of 1-100 nm while Nanotechnology refers to the study and manufacturing of materials at atomic and subatomic level. About 50 years ago, Nobel Laureate in Physics Richard P. Feynman is considered as father of Nanotechnology as he gave the concept of Nanotechnology and Nanoscience in his lecture entitled "*There is plenty of room at the bottom*". Later on, In 1974 Professor N. Taniguchi introduced the term "nanotechnology" [1].

1.1.1. **Classification of Nanomaterials.** Nanomaterials can be classified on the basis of dimension and composition. Siegel had classified nanomaterials in following categories on basis of dimension.

a) *Zero Dimensional (0-D).*This type of nanomaterials have all dimensions in nanometer (nm) range. Mostly they are spherical in shape e.g. Nanodots, clusters etc.

b) *One Dimensional (1-D).*In 1D nanomaterials only 1 dimension is out of nm range. They are long like cylinders e.g. nanorods, ribbons, nanotubes and fibers etc.

c) *Two Dimensional (2-D).*These nanoparticles are just like sheet with two dimensions out of nm range e.g. coatings, Films etc.

d) *Three Dimensional (3-D).* Large materials with no dimension in nanometer range are categorized in 3D nanomaterials e.g. polycrstals and sand etc. [2].

Figure 1.1 demonstrates the examples of Siegel's classification of nanomaterials.

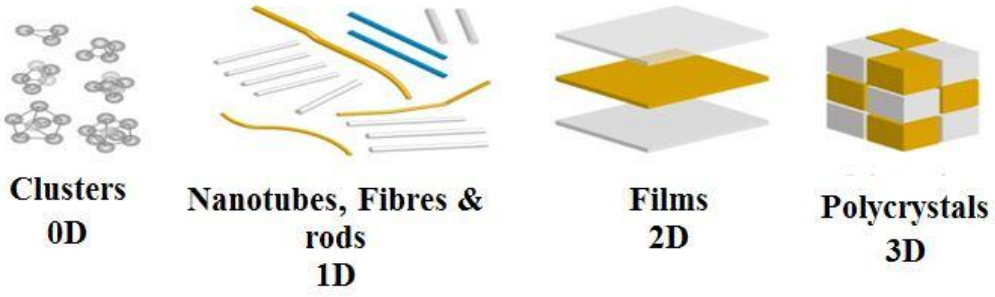

Figure 1.1. Classifications of nanomaterials on basis of dimension [3]

On basis of composition following are types of nanomaterials.

a) *Carbon based Nanomaterials.*

b) Metal based Nanomaterials.

c) Dendrimers.

d) Composites.

*a. Carbon based Nanomaterials***.** These nanomaterials are mainly composed of carbon. They may be in form of hollow tube, ellipsoidal and sheets. For example Fullerenes, Carbon nanotubes, Graphene as shown in figure 1.2.

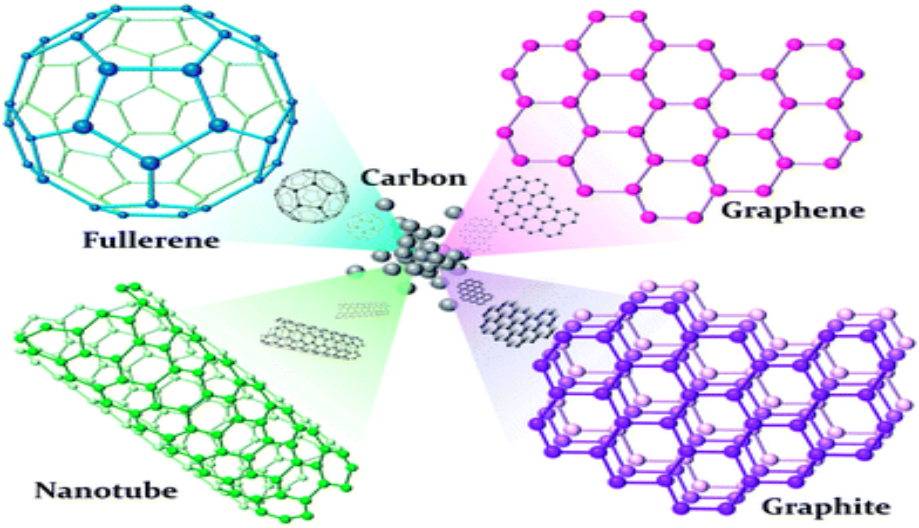

Figure 1.2. Classifications of nanomaterials on basis of composition [4]

b. Metal based Nanomaterials. Metal nanoparticles are the main component of metal based nanomaterials. For example quantum dots, Au nanoparticle, Si nanowires etc.

c. Dendrimers. The term dendrimer is originated from Greek word “dendra” meaning “Tree”. They are basically nanopolymers and offer high surface functionality and versatility due to their highly branched 3D structure.

d. Composites. Composites are unique materials that are originated from combination of nanoparticles and other materials like ceramics, metal or polymer matrix. Here one of the material is called reinforcing phase and other one is called matrix phase in which reinforcing phase in form of particles or sheets is embedded [5].

1.1.2. Synthesis of Nanomaterials. Generally two approaches are used to synthesize nanomaterials, *a). Top down approach.* In top down approach smaller materials are synthesize from large initial structures. It involves breaking down of large materials into smaller particles and *b). Bottom up approach*. In this technique materials and devices are built from smaller components (atoms, molecules) [6].

1.2. Ferrites.

Ferrites are considered as one of the most important class of ceramics with magnetic properties as they contain iron oxide as a main component. The history of ferrites began over 1000years ago. Like in 2600 BC, magnetite was used in navigation as compass by one of the Chinese empire 'Haung-Ti' [7]. Later on, synthesis and then correlation of magnetic properties with chemical composition of spinel ferrites was done by Hilpert for the first time. These spinel ferrites have general formula MFe_2O_4 (M=Divalent metal ions like Ni, Ca, Cu, Zn etc.) [8]. Kato and Takei who was the Japanese researchers have also major contributions in the field of ferrites. Like their 1^{st} discovery was higher magnetization of both cobalt ferrite and magnetite solid solution at room temperature while they show poor magnetization at higher temperature i.e.300ºC [9]. Moreover the discovery of magnetic core materials was also done by them. These important discoveries enabled scientist to use ferrites based materials in electronic industries. In 1945 Neel gave the concept of ferrimagnetism and magnetic behavior of ferrites [10].

1.2.1. Classification of Ferrites. On basis of Magnetic behavior ferrites can be classified as hard and soft ferrites.

a. Hard Ferrites. They are also known as permanent magnet as they are hard to magnetize and then demagnetize. They have high saturation magnetization and coercivity (Figure 1.3) .Hard ferrites have hexagonal structure and are mainly composed of Fe and Ba or Sr oxides [11].

b. Soft Ferrites. They are known as soft ferrites owing to their property to magnetize and demagnetize easily. They have small coercivity values as shown in figure 1.3 so

they can act as magnetic field conductors. They are mostly composed of nickel, manganese and zinc compounds [12]. Hysteresis loop for soft as well hard ferrites is shown in figure 1.3.

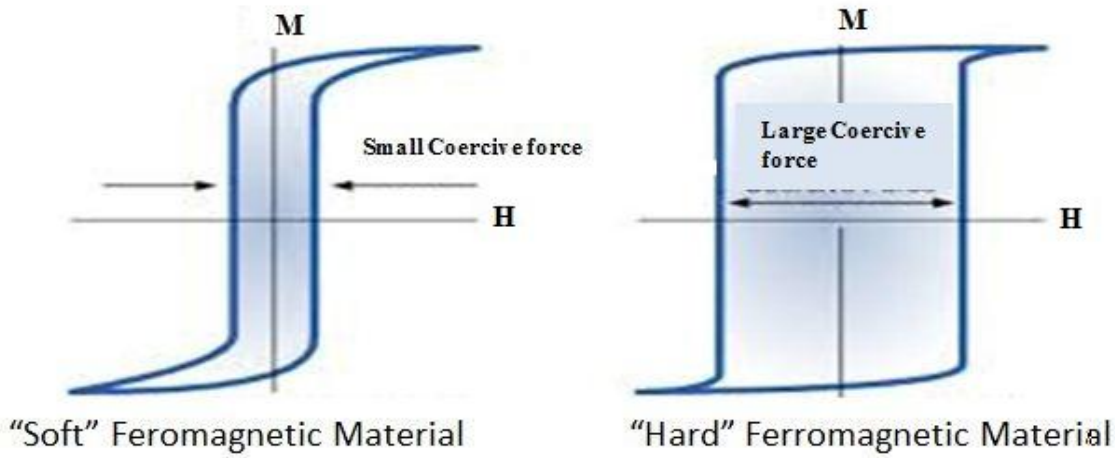

Figure 1.3. Hysteresis loop for soft and hard ferrites [13]

1.2.2. Advantages of Ferrites. Following are the advantages of Ferrites.

- Higher resistivity
- Broad frequency range (10 kHz to 50 MHz).
- Cost effective.
- Economically assemble.
- Stability of time and temperature [14].

1.2.3. Applications of Ferrites. Production of FNPs is becoming one of the fascinating areas of research owing to their applications in almost every field of life such as in electronic devices for energy storage applications, have antimicrobial activity [15], biomedical application like magnetic resonance imaging (MRI), hyperthermia, drug delivery etc. [16], [17] used as sensors for different poisonous gases [18]. It has also contributed a lot in waste water treatment by acting as a photocatalyst [19]. Figure 1.4 shows the hierarchal diagram for few applications of ferrite nanoparticles.

1.3. Spinel Ferrites.

Spinel ferrites are a large group of materials and have general formula AB_2O_4 (A=Divalent metal ion like Ni^{2+}, Co^{2+}, Mg^{2+} B=Trivalent metal ions mostly iron) and have similar structure of natural spinel $MgAl_2O_4$.

1.3.1. Classification of Spinel Ferrites. Spinel can be classified into following types on the basis of cationic distribution on tetrahedral or octahedral sites figure 1.5 shows the crystal structure of spinel ferrites in which octahedral (B) and tetrahedral sites (A) are present.

1.3.1.1. Normal Spinels**.** Their general formula is (M_1^{2+}) $[Fe^{3+}]_2O_4$. In normal spinels tetrahedral or A sites are occupied by divalent ions while trivalent ions are present at octahedral or B sites.

1.3.1.2. Inverse Spinels. They have general formula (Fe^{3+}) $[M_1^{2+}Fe^{3+}]O_4$. Here divalent metal ions are present at B site while trivalent metal ions are present either in B site or A site.

1.3.1.3. Mixed Spinels. Mixed spinels consist of divalent metal ions present in both A and B sites and have no definite preference. Spinel ferrites have various applications in the field of drug delivery, antibacterial activity, gas sensors, energy storage devices and microwave devices [21].

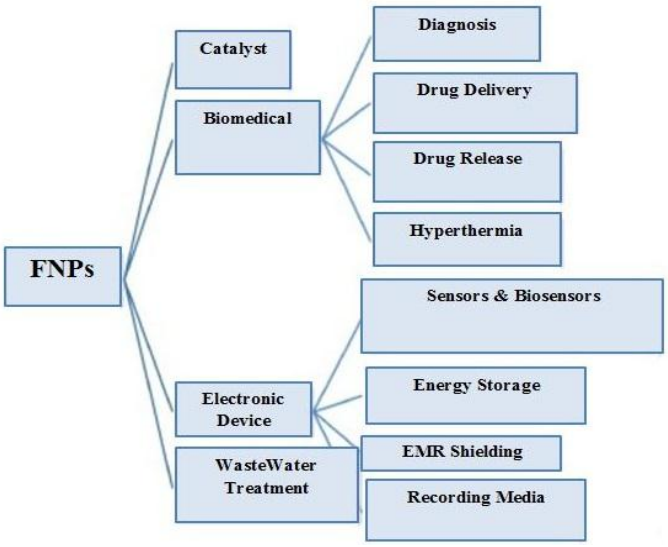

Figure 1.4. Application of ferrite nanoparticles [20]

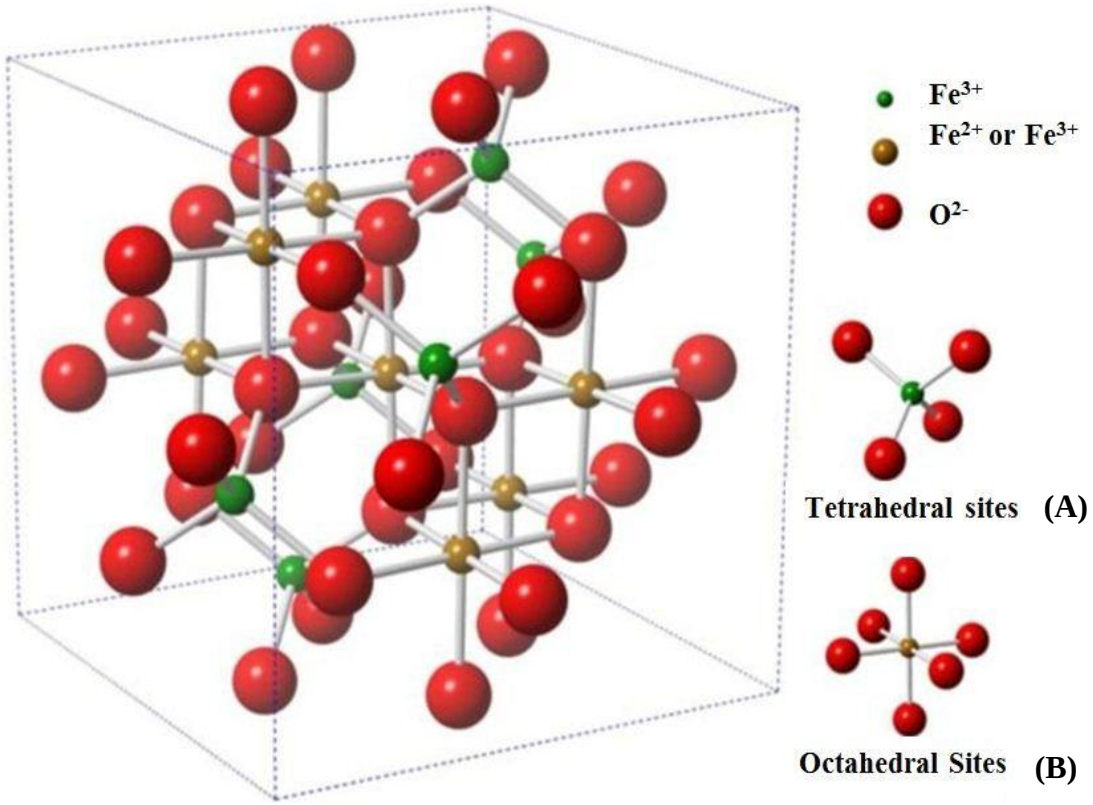

Figure 1.5. Crystal strucutre of spinel ferrites [22]

1.3.2. Properties of Spinel Ferrites. Spinel Ferrites have various properties like magnetic, electric, dielectric and optical properties etc.

1.3.2.1. Magnetic Properties. Feri and ferromagnetic materials show similar net magnetization but the difference between them arises due to alignment of metal ions spin moments. Spins are aligned anti parallel for ferrimagnetic materials while for ferromagntic materials the alignment of spins is parallel as shown in given figure 1.6.

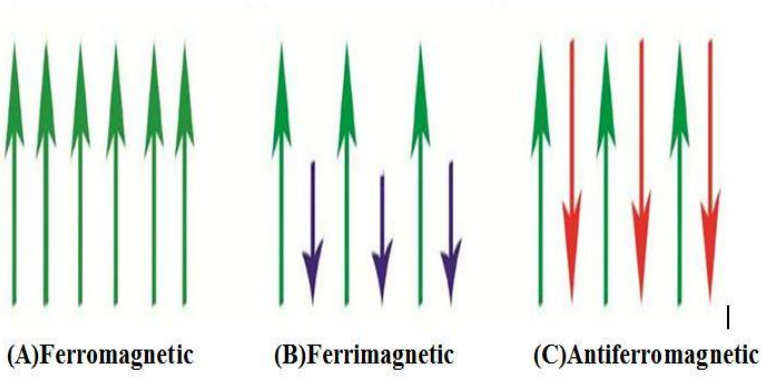

Figure 1.6. Magnetic behavior of Ferromagnetic (A), Ferrimagnetic (B) and Antiferromagntic materials(C) [23]

In addition, the magnetism in ferromagnetic materials can also be explained by the presence of spin magnetic moment of transition metal 3d unpaired electrons and their

interactions through oxygen ions present between. The strength of exchange interactions between magnetic moment of metal ions depends upon various parameters like distance as well as angle of metal ions and presence of oxygen ions between them. The A-O-A and B-O-B interactions are much weaker than A-O-B interactions in inverse spinels. Hence the ferromagnetic behavior is due to coupling in magnetic moment of metal ions within sublattices on both octahedral and tetrahedral sites while antiferromagnetism is based on coupling of magnetic ion moments between sublattices. But sometimes there is a possibility of presence of all ferromagnetic as well as antiferromagnetic order, spin glass behavior, local spin canting etc. due to topological frustration arises from presence of competing exchange interactions on magnetic ions at both sites. In case of nickel ferrite half of Fe^{3+} present in A site and remaining half are present at B site along with all Ni^{2+} ions. Hence magnetic moment of iron ions at both site is cancelled as they are antiparallel to each other so net magnetization is due to presence of nickel ions. Moreover the magnetic behavior of ferrites also depends on temperature and particle size [24].

1.3.2.2. Dielectric properties. Dielectric materials are the poor conductors of electricity or are insulators due to presence of strong attractive forces between their constituents and also due to absence of free electrons. But dielectric polarization can be produced by applying electric field. As shown in figure 1.7 positive ions aligned themselves in direction of electric field while negative ions are present opposite to applied field resulting weak field is produced opposite to applied field [25].

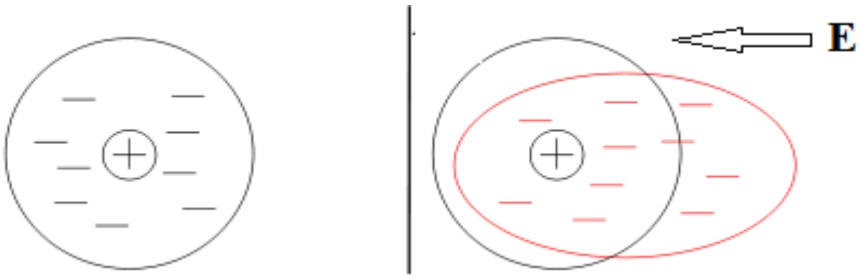

Figure 1.7. Interaction of atom with applied electric field.

In this way capacity of dielectric materials to store energy is enhanced as compared to vacuum that causes increase in per unit voltage capacitance of capacitors known as relative permittivity or dielectric constant. Common types polarization induced in dielectric materials as response to applied electric field are depicted in figure 1.8 and are Dipolar, electronic, Ionic and space charge polarization. All these polarization occurs at different frequency range means these all are frequency dependent.

Orientation of polar molecules in presence of applied field termed as orientation or dipolar polarization. It may sometimes inherently present in molecules. Electronic polarizations are due to dislocation of nucleus w.r.t. neighboring electrons in neutral atoms while, ionic polarization in ionic solids comprises the alignment of opposite ions [26].

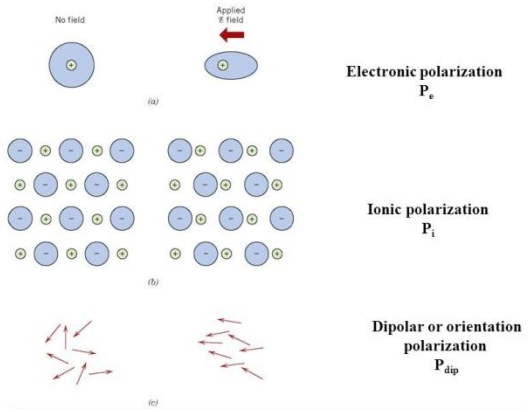

Figure 1.8. Types of polarization [27]

1.3.2.3. Magnetic Properties. The physical phenomenon due to movement of electrical charges or as a result of force exerted by magnet is known as magnetism [28]. Generally in order to understand the magnetic properties of materials hysteresis loop is drawn that shows relationship between induced magnetic field and applied field. It is also known as B-H loop. By changing the magnetizing force magnetic flux of magnetic materials is recorded then this data is used to generate hysteresis loop. Figure1.9 shows the hysteresis loop for magnetic materials. The dashed line in loop represents the behavior of ferromagnetic material that may be either demagnetize thoroughly or not magnetized by increasing applied field. In addition, it also shows that magnetizing force is increased by increasing applied current or field. By increasing the point is reached at which alignment of all magnetic domains has been done. This point is known as Saturation Magnetization. Point 'a' represent the saturation magnetization point. After this point the magnetizing force has not affected the flux density (magnetic field). Then by reversing the direction of force the curve move from point a to b. This point demonstrate that although force is zero but still there is some magnetic flux present in material so this point refers as retentivity or remanence point (point at which some magnetic domains are in alignment but some domains lost their alignment). By further applying force but in opposite direction the curve reaches to point of coercivity (magnetic flux=0) while the force applied to remove the residual magnetism of materials is known as coercive force. Now, for

further increasing the force in negative direction same trend is followed for saturation magnetization, retentivity and coercivity in opposite direction to complete loop.

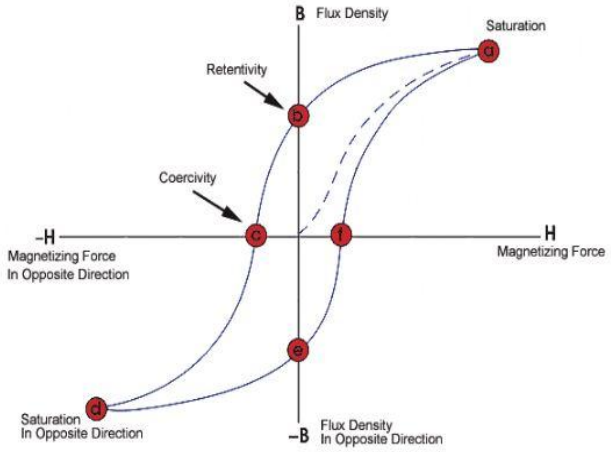

Figure 1.9. Hysteresis loop for magnetic materials [29]

1.3.3. Nickel Ferrite. Nickel ferrites have inverse spinel crystal structure as Ni^{2+} present in B site while Fe^{3+} present in both A and B sites. Due to magnetic moment of antiparallel spins of these metal cations nickel ferrites are ferrimagnetic in nature. Nickel ferrite is considered as soft magnet due to its low coercivity, low eddy current losses and low hysteresis loss at high frequency [30]. The electrical, magnetic and structural properties of nickel ferrites depend on occupancy of tetrahedral and octahedral sites and also on synthesis method [31].

1.4. Characterization Techniques.

Following techniques are used to characterize synthesized nanoparticles.

1.4.1. X-Ray Diffraction (XRD). XRD is a nondestructive technique mainly used for phase identification, crystal structure, texture and crystal defects of crystalline materials on unit cell dimension. The X- ray phenomenon was discovered by German physicist Max von Laue and Co in 1912 and they suggested that atomic spacing of crystal lattice are small enough to create diffraction pattern by X-rays [32].

1.4.1.1. Principle of XRD. The basic principle behind XRD is constructive interference of crystalline sample and monochromatic X-rays. The constructive interference is produced when incident rays fall on sample if conditions fulfill Bragg's Law.

$$\mathbf{n\lambda = 2d\sin\Theta}$$

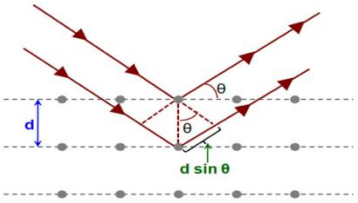

Figure 1.10. Schematic diagram for Bragg's law [33]

Bragg's law gives relationship between the wavelength of X-rays to the diffraction angle and the lattice spacing (d) of crystalline sample. According to this law if two parallel incident X-rays make an angle (Θ) with atomic planes and when these rays are reflected they will interfere constructively only if the distance covered by these rays is integral multiple of their wavelength (nλ).

1.4.1.2. Working of XRD. X-ray diffractometer includes following main components:

- X-Ray tube or Cathode ray tube (CRT).
- Sample holder.
- Detector.

X-ray tube consists of heated filament for production of electrons. These electrons are accelerated towards target (Cr, Mo, Fe etc.) by giving them voltage. If these electrons have enough energy to remove the inner shell electrons of that target then polychromatic X-rays are produced. These X-rays are directed towards sample after filtering them by monochromators as shown in figure 1.10. The intensity of diffracted X-rays in form of peaks is recorded by detector. The results are obtained as the output to device such as monitor or printer [34].

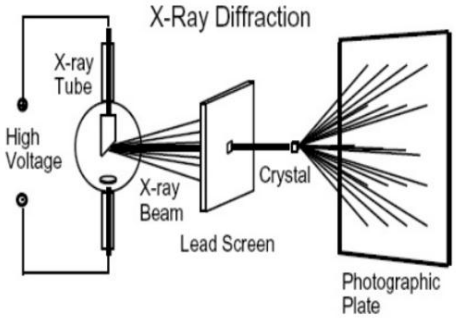

Figure 1.11. Schematic representation of X-Ray Diffraction [35]

1.4.1.3. Limitations of XRD. Following are limitations of XRD.

i. Sample must be homogenous and single phase material for characterization.

ii. The detection limit for mixed materials is approximately 2%.

iii. Minimum amount of sample required for characterization must be in tenths of gram.

XRD have several advantages over other techniques like it is nondestructive technique and can have ability to determine purity and unit cell dimensions of unknown crystalline materials.

1.4.2. Scanning Electron Microscopy (SEM). Scanning electron microscopy is one of the most important characterization technique used to get information about morphology, topology, phase distribution and composition of sample. McMullan introduced SEM for the 1st time while Manfred von Ardenne prepared first microscope [36]. A beam of electrons is used in SEM to get image of object. Resolving power of SEM is much more than ordinary electron microscope because incident beam of electrons is less converging and have larger depth of focus that can cover whole sample and as a result sharp 3D image of sample is obtained [37]. Depth of focus and image formation in both optical as well as scanning electron microscope is well illustrated in figure 1.12.

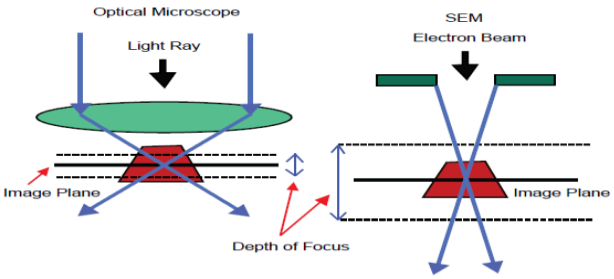

Figure 1.12. Image formation in optical microscope vs Scanning electron microscope [38]

1.4.2.1. Construction and Working of SEM. Components of scanning electron microscopy are:

i. Electron Gun.

ii. Thermionic electron gun (Electron emitted from heated filament)

iii. Field emission electron gun (Electron emitted from sharp tip using electric field Magnetic lenses.

In SEM electrons are produced by electron gun that are accelerated by applying high potential then these accelerated electrons are focused on sample using a pair of

electromagnetic lenses. The scanning coils are used to scan the electron beam over the surface of sample. The signals produce as a result of interaction of electron beam and sample are measured by detector [39]. Figure 1.13 represents the phenomenon of image formation by SEM.

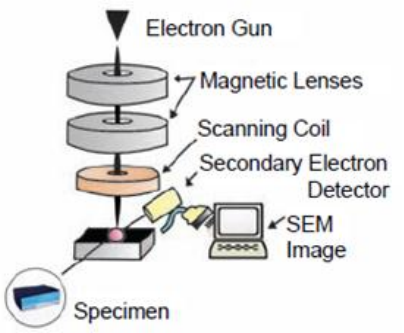

Figure 1.13. Image formation in SEM [40]

1.4.2.2. Principle. Different types of signals produced as a result of interaction of electrons with atoms of sample at different depths which are given below.

- Backscattered electrons (BSE).
- Auger electron.
- Cathode luminescence (CL).
- Secondary electrons.

If the incident electrons beam interact with atoms of sample and eject electrons from usual orbits then these electrons are known as secondary electrons (Elastic collision) and these electrons are the most common source for imaging of sample because they are large in number produce as a result of chain reaction taking place by incident beam. Secondary electrons are used to give topographical information of sample. In contrast to secondary electrons, Backscattered electrons are produced when incident electrons strike nuclei of atom and bounce back (Inelastic Collision). These electrons are higher in energy and give information about difference in the densities of sample as the electrons are produced from depth of sample so images of atoms with higher atomic numbers appear brighter than that of images of lower atomic number atoms. But a single machine could not detect all types of signals produced as a result of SEM [41]. Different types of detectable signals produced as a result of bombardment of electrons on sample are mentioned in figure 1.14.

1.4.2.3. Preparation of Sample. For SEM analysis the sample should have following requisites.

- It should be conductive and flat
- Have appropriate size
- Surface of sample should be exposed
- Can tolerate under vacuum condition [42].

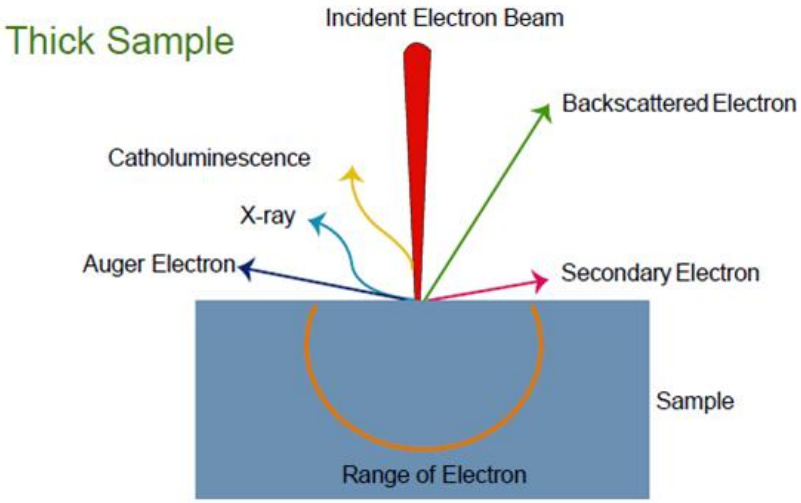

Figure 1.14. Schematic Diagram for interaction of electron beam and sample

1.4.3. Energy Dispersive X-Ray Spectroscopy. EDX is one of the best techniques for elemental detection and is used as an extension to other analytical techniques like SEM and TEM. For elemental detection it requires emitted X-ray spectrum of sample.

1.4.3.1. Principle. When a high energy electron beam is bombarded onto the sample elastic as well as inelastic collisions take place resulting in knock out of certain electron and vacancy/hole is created. These holes are then filled by higher orbital electrons resulting emission of characteristics X-rays. Figure 1.15 demonstrates the phenomenon of X-Rays emission by bombardment of electrons.

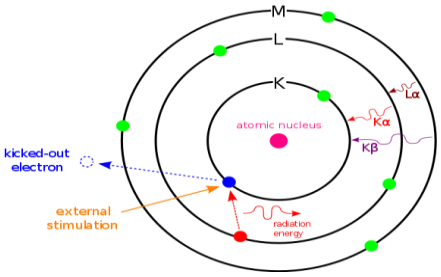

Figure 1.15. Phenomenon of X-Rays emission [43]

1.4.3.2. Construction and working of EDX. EDX consists of following main parts.

- Source.
- Detector.
- Processor.
- Analyzer.

Characteristics X-rays emitted by Electron beam (SEM, TEM) and X-rays (XRF) are used in EDX. Theses X-rays are sent to detector where these X-rays are converted into signals of voltage, processed by pulse processor and then analyzed and displayed by analyzer. The most commonly used detectors of EDX are silicon drift detectors and Si (Li) detector [44]. Schematic representation of EDX is given in Figure 1.15.

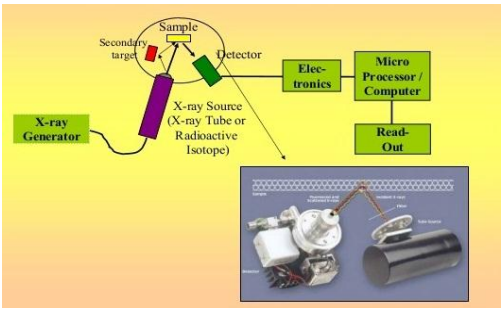

Figure 1.16. Schematic representation of EDX

EDX have various advantages as it is extension to SEM so no large setup is required for it. It can identify all elements ranging from Be(4) to U(92). In addition, EDX can provide facility of fast analysis both for quantitative and qualitative aspects [45].

1.5. Optical Properties.

Band gap is measured by UV-Vis spectrophotometer.

1.5.1. Ultraviolet-Visible Spectroscopy (UV-Vis). UV-Vis states to the spectroscopy related to the absorption some time also refer to reflectance spectroscopy depending

on the mode of use which a UV-Vis device contains. All these type of the phenomenon occurs in the range of 200 nm to 800 nm of wavelength. Different chemicals absorbs or reflect at different wavelengths of the light so this property helps for the UV-VIS characterizations. In UV-Vis region of electromagnetic spectrum molecules or atoms shows the process of electronic transitions. Absorption spectroscopy sometimes also refer to the fluorescence spectroscopy in that fluorescence contracts with transition process in which electron jumps from ground state to the excited state. UV-Vis also used to identify the kinetics or also rate constant of a under observation chemical reaction. Color or brightness shift must be occurred during chemical reaction from reactants to the products for the perfect use of UV-Vis. Other interesting application of this technique is that we can easily calculate the band gap of materials or composites. For this purpose we use the following mathematical formula.

$$\mathbf{E_g = hc/\lambda}$$

Here E_g is the band gap energy, *h* is the Planck's constant and λ is the wavelength [46].

1.6. Dielectric Properties.

In order to observe dielectric properties LCR meter was used.

1.6.1. LCR Meter. LCR is a type of electronic device that is used to find the impedance of a device or a circuit that is created by means of alternating current. LCR meter is actually a multimeter as it can measure inductance, Capacitance and Reactance by converting the values of impedance.

1.6.1.2. Types of LCR Meter. Commonly, there are two types of LCR meter**.**

a. Hand held. As name indicates this type of LCR meter is light in weight so it is portable .It has ability to measure AC resistance and Inductance providing accuracy ranging from 0.2% to 0.1% held LCR meter**.**

b. Bench Top. Bench top LCR meter is large in size that's why it is fixed at certain position. It provides several advantages like it can measure DC bias voltage, sweep and current with higher frequency (0.01 %). Moreover frequency have programmable settings.

1.6.1.3. Working Principle. By passing the AC voltage through device under test (DUT) current, voltage and phase angles are measured in LCR meter. These measured factors are then used to calculate all impedance parameters.

1.6.1.4. Techniques used in LCR meter**.** Mostly two techniques are used in LCR meter.

a. Wheatstone Bridge. This method is used to measure low frequencies upto 100Hz by placing the DUT in a bridge.

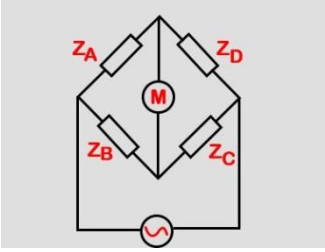

Figure 1.17. Circuit Diagram of Wheat stone Bridge

Impedance of DUT is measured at a point when all the components in wheat stone bridge are balanced. According to figure 1.16. Z_D is an impedance of DUT and Z_A is changeable as long as no current flows through Z_D while Z_B and Z_C have known values of impedance .At balance position of bridge all components obey following equation [47].

$$\boldsymbol{Z_D/Z_A=Z_C/Z_B}$$

So impedance of DUT can be calculated as

$$\boldsymbol{Z_D=Z_C/Z_B\times Z_A}$$

b. Current voltage measurement technique. In this technique impedance of DUT is measured by measuring the values of current and voltage .Here ammeter and voltmeter arrangements are used to measure low impedance and high impedance current respectively and then results are shown in terms of resistance, Capacitance and inductance [48].

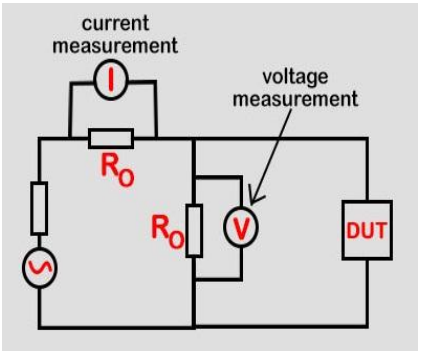

Figure 1.18. Circuit diagram of current voltage measurement technique

1.7. Magnetic Properties.

Magnetic properties was determined by Fluxgate DC magnetometer.

1.7.1. Fluxgate Magnetometer. Magnetometers are instruments that are used to measure magnetism in magnetic materials. In 1936 Fluxgate magnetometer was invented. These are used to sense magnetic field in highly precise manner.

Principle. DC current is used to derive core of fluxgate magnetometers by saturating it. Then by change in current in outer coil facilitates the detection of external magnetic field by AC offset proportional to magnetic field strength. Finally, magnetic field signals are extracted by phase demodulation circuitry. Figure 1.18 shows the schematic diagram of DC magnetometer [49]

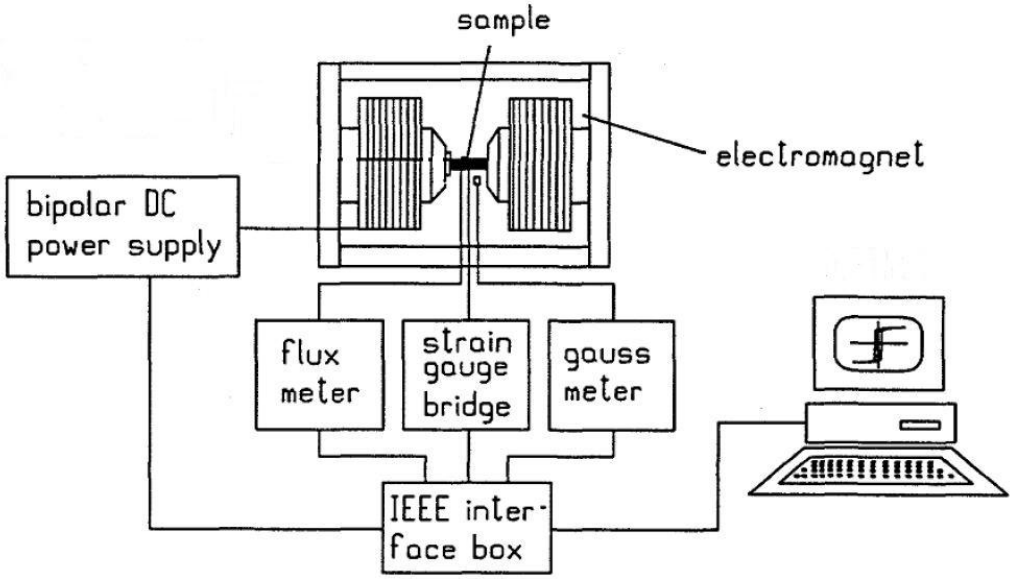

Figure 1.19. Schematic diagram of DC Magnetometer [50]

Chapter 2

Literature Review

This chapter is about synthesis and properties of spinel ferrites and alkaline earth metals doped spinel ferrites nanoparticles. Most specifically alkaline earth metals doped transition metals ferrites nanoparticles.

2.1. Crystal Structure of Spinel Ferrites.

Spinel ferrites are large group of materials having same structure as natural spinel $MgAl_2O_4$. They have natural tendency of incorporating different charge bearing cations into their structure so they are present in large variety. But in order to incorporate cations it must be noted that positive charge should be less than 8 that is necessary to balance anions and also cation radii should be ranging from 0.4-0.9Å [51].

The general formula of magnetic spinels commonly known as Ferrites is MFe_2O_4 (M=Divalent metal ion). One of the most significant and abundant is the natural Fe_3O_4 (Hematite) [52]. In 1915 Bragg investigated the crystal structure of spinel ferrites for the first time. The structure of spinel ferrites contains metal ions that are coordinated to oxygen in two different symmetries and as a result generating two coordination sites named as A site (Tetrahedral Symmetry) and B site (Octahedral symmetry) [53]. Spinel Ferrites are existed in form of cubic unit cell with space group Fd3m. The literature study showed that each unit cell of spinel ferrites contain 8 units AB_2O_4 and total 56 ions [54].

2.2. Synthesis of Spinel Ferrites.

Up to Now, Lots of spinel Ferrites have been prepared by wet chemical and solid state synthesis methods. Dong-Hwang Chen et al reported the synthesis of nickel ferrite nanoparticles via sol gel route in the size range 5-30nm. Beside other precursors polyacrylic acid was used in reaction that acted as chelating agent and also help to improve crystallinity of nanoparticles by providing combustion heat [55]. M. Atif et al in 2006 synthesized zinc ferrite nanoparticles in two different media i.e. acidic and basic by sol gel method and then studied the effect of medium on magnetic

properties and particle size. The results of different characterization techniques revealed that samples prepared in basic media had smaller particles size and were more ferromagnetic in nature [56]. M. Santii prepared the inverse spinel Ni-Ferrite nanoparticles using egg white and metal nitrates. The advantage of this method was that there was no need of pH adjustment throughout the reaction. They have reported that obtained nanoparticles have size 60-600nm [57]. Later on, co precipitation method was employed by K. Maaz et al to obtain single phase nickel ferrite nanoparticles using oleic acid as surfactant. The size of nanoparticles was directly related to annealing temperature while coercivity value of sample were increased upto particles having size 11nm and then decreased as the particles size were further increased [58]. In the same year solvothermal method was used to synthesize nanoparticles of nickel ferrite using ethylene glycol and sodium acetate as solvent and stabilizing agent respectively. The size of resulting nanoparticles were easily controlled by varying reaction conditions like time duration of reaction, amount of stabilizing agent etc. VSM results showed that synthesized ferromagnetic nanoparticles were ferromagnetic in nature and can be used in biomedical applications [59]. N. Rezlescu et al in 2012 synthesized Ni, Cd, Cu and Zn ferrite nanoparticles using auto combustion method. They used polyvinyl alcohol to make sol of metal precursor's solution. Ammonium hydroxide was used to maintain required pH resulting formation of gel followed by drying and sintering as a result desired nanoparticles were obtained [60]. In the same year copper ferrite nanoparticles were prepared by S.Singh et al via co-precipitation method using metal chlorides as precursors of reaction and then study their response as LPG sensing application after making pallets of product .The results showed that product containing copper and iron in 1:1 had best gas sensing response [61]. Kamellia Nejati and Rezvanh Zabihi synthesized nickel ferrite nanoparticles via hydrothermal method in order to study the effect of Glycerol or Sodium dodecyl (Surfactants) on the size of nanoparticles. The prepared nanoparticles were then characterized by XRD, TEM, FT-IR and VSM. It was inferred from the results that surfactant assisted produced nanoparticles had smaller in size (10-15nm) and were uniform but the crystallinity of particles were reduced [62]. In the very next year, Sonochemical method was used by P. Partha and Goswam et al to synthesize cobalt ferrite nanoparticles and in order to obtain required nanoparticles the overall reaction was completed in 3 steps i.e. hydrolysis of precursors followed by oxidation and calcination [63].

2.2.2. Alkaline Earth Metals Doped Ferrites. In 2001 H. M.Widatallah et al. prepared magnesium substituted lithium ferrite nanoparticles via simple sintering process. First of all they synthesized magnesium doped alpha-Fe_2O_3 by hydrothermal method and then ground them with lithium carbonate in pestle and mortar and finally ground powder was placed in furnace at 600°C. The lattice parameters and magnetization of prepared nanoparticles were increased due to larger ionic radii of magnesium [64]. After few years, A.A.Sattar et al used ceramic method to synthesize calcium doped lithium zinc ferrite. Metal oxides used as precursors were mixed together and then placed in muffle furnace at 800 degree centigrade for pre sintering the product was then ground in pestle and mortar and then pallets were formed by applying high pressure .These pallets were finally sintered to obtain desired product. Saturation magnetization (upto x=0.01), lattice parameters, coercivity and remanence ratio of product increased while permeability decreased with increasing doping concentration [65]. In 2009 B Bhushan et al reported thermal electrical and magnetic properties of bismuth ferrite after doping different alkaline earth metals (Ba, Sr & Ca). The results of different characterization tools showed that doped nanoparticles have decrease in Neel temperature while they have increased in band gap. Magnetic studies revealed that nanoparticles were weak ferromagnetic in nature [66].

In 2011 M. K. Shobana successfully synthesized calcium substituted nickel ferrite nanopowder via sol gel autocombustion route having particle size 70-90nm [67]. In 2012 Refka Andoulsi et al synthesized Calcium doped Lanthanum ferrite nanopowders by polymerizable complex method. The results of different characterization techniques like XRD, SEM, FTIR and CIA indicated that no structural and morphological changes took place by Ca doping. However their electrical conductivity varied directly to calcium ion concentration [68]. In 2012 B.Bhushan et al reported that how calcium and barium co doping effect the magnetic and optical properties of bismuth ferrite nanoparticles. Optical studies showed that band gap was increased upto 0.5ev similarly increase in saturation magnetization and coercivity were also observed when there were equal concentration of both dopants [69]. A.Manikandan et al in 2013 synthesized spherical shaped magnesium doped zinc ferrite nanoparticles via microwave combustion method using metal nitrates as precursors and urea as fuel. The synthesized nanoparticles have size ranging from 15-43 nm. They reported that by increasing magnesium concentration crystallite size decreases due to small radii of metal cation. VSM and PL spectrum showed that

magnesium doping had direct effect on magnetization while value of band gap decreased as the magnesium concentration increases [70]. In the same year Sunil Chauhan et al synthesized barium doped bismuth ferrite nanoparticles by sol gel method using metal nitrates as precursors and reported morphological and structural changes occurred by changing concentration of barium. All the synthesized nanoparticles were ferromagnetic in nature [71].

In 2014 D. Gherca et al investigated the properties of nanopowder of cobalt, magnesium, manganese and nickel ferrite prepared by ecofriendly coprecipitation method using canola oil as capping agent in order to avoid agglomeration and metal chlorides as precursors of reaction. The synthesized nanoparticles were then investigated by VSM, SEM and XRD and their results showed that nanoparticles were spherical in shape with their grain size~10nm [72]. A.Chaudhuri and Mandal prepared barium doped bismuth ferrite nanoparticles via hydrothermal method and characterized them by XRD and FESEM. The change in various properties took place after doping like enhancement of magnetization, remnant polarization, energy of activation and dielectric constant shown by results of characterization techniques. Moreover the efficiency of prepared sample as dielectric material is directly related to energy of activation [73]. In the same year K. K. Bamzai et al reported the synthesis of calcium doped Mg-Ferrite via ceramic method and then analyzed their structural and magnetic properties by varying chemical composition. Characterization of sample was done by XRD, EDX and SEM. The results of these techniques showed that prepared sample have cubic spinel structure and had maximum Curie temperature when composition was $MgFe_2O_4$. The prepared sample can be used in various applications like sensors, color imaging, microwave absorbents etc [74]. G.D.Poonam and N.K.Verma synthesized Ba doped Bismuth ferrite nanoparticles ($Bi_{1-x}Ba_xFeO_3$ x=0 & 0.15) by using Sol-gel method and analyzed the effect of prepared nanoparticles size on the electrical, magnetic & dielectric properties. The particles size was varied by varying calcination temperature .The prepared nanoparticles was then characterized by using XRD, TEM, SEM and DSC revealed that prepared sample has rhombohedral structure and have larger values of saturation magnetization & dielectric constant after Ba doping & when particle size is small hence by decreasing particle size multiferroism of Ba-doped $BiFeO_3$ particles had increased [75]. In 2015 K.Nadeem et al reported the synthesis of magnesium doped zinc ferrite nanoparticles by co precipitation method and studied the effect of annealing on

prepared nanoparticles .Annealing had direct effect on structure of particles as crystallite size and particles both increased by annealing that was confirmed by XRD and SEM while VSM showed that magnetization as well as coercivity both decreased by annealing due to rearrangement of cations at coordination sites [76]. H.Moradmard et al reported the synthesis of Mg- doped Ni-ferrite Nanoparticles having general formula $Ni_{1-x}Mg_xFe_2O_4$ by co-precipitation method and then analyzed them by XRD, EDX, FTIR, FESEM and VSM. which confirmed that prepared sample have single phase inverse structure and have ferromagnetic behavior .By increasing concentration of Mg^{2+} crystallite size and lattice constant also changed similarly value of saturation magnetization decreases while coercivity (Hc) increases was due to replacement of Fe^{3+} by Mg^{2+} as magnesium ion have larger ionic radius .The prepared particles can be used in ferrofluids, microwave devices, gas sensors and magnetic applications [77]. In 2016 V. Srinivas1, et al, synthesized Ba doped bismuth ferrite nanopowder using different concentration of Ba via sol gel method and then analyzed the effect of Ba ion concentration on various properties of sample .The prepared sample was characterized by XRD, SEM and VSM and their results showed that increase in Ba concentration caused increase of magnetization and lattice parameters and also change in structure of prepared sample [78]. Later on, Hirthna & S.Sendhilnathan synthesized Mg doped Ni-ferrite nanoparticles via Co-precipitation method with average particle size 28nm-10nm obtained by Debye-Scherer formula. They used different analytical techniques like XRD, TEM and FESEM to observe the properties of prepared sample and their results showed that particles have spinel structure and super paramagnetic in nature. They reported that values of magnetic saturation and conductivity varied directly while dielectric loss as well as dielectric constant values of prepared nanoparticles were inversely related to Mg concentration [79]. In 2017 H.S.Mund and B.L.Ahuja successfully abled to synthesize spinel structured Mg doped cobalt ferrite nanoparticles via sol-gel combustion method. Spectral analysis via XRD, FTIR and Raman showed that after doping magnesium parent hard ferrite converted into soft ferrites which altered its properties .Similarly by changing Mg concentration various properties like saturation magnetization, frequency bands shift and magnetic moment also changed [80]. Then in the same year T.Vigneswari and P.Raji synthesized calcium doped Ni-Ferrite nanoparticles by co-precipitation method using different concentrations of calcium .and then prepared nanoparticles were characterized by FESEM, XRD, ICP, VSM, XRD and FTIR analysis indicated that

nanoparticles have single phase inverse spinel structure with crystallite size in range of 22-34nm .The magnetic properties of prepared nanoparticles had influenced by calcium concentration i.e. saturation magnetization increased upto x=0.2 and then decreased gradually. The calculated squareness ratio for prepared nanoparticles was 0.115-0.435 that indicated that prepared nanoparticles can be used in memory core devices [81]. Pradeep Chavan and L. R. Naik investigated the optical and structural properties of magnesium substituted nickel ferrite nanoparticles synthesized by easy and simple autocombustion method .The average particles size as well porosity of prepared nanoparticles were increased by increasing doping concentration. The band gap measured by Tauc plot was also increased but decrease in DC electrical resistivity w.r.t temperature showed that nanoparticles were of semiconducting in nature [82].

.

CHAPTER 3

Experimental

This chapter comprises of nickel Ferrite nanoparticles, Barium Ferrite nanoparticles and Barium doped Nickel Ferrite ($Ba_xNi_{1-x}Fe_2O_4$) nanoparticles synthesis via hydrothermal method. Nickel (II) Chloride hexahydrate ($Cl_2Ni.6H_2O$), Barium Nitrate [$Ba(NO_3)_2$], and Ferric chloride hexahydrate ($FeCl_3.6H_2O$) was used as precursors while NaOH was used as precipitating agent. All the chemicals were of analytical grade and purchased from Sigma-Aldrich with ~99% purity.

3.1. Synthesis of Nanoparticles.

Hydrothermal method was adopted to prepare nickel ferrite and barium ferrite nanoparticles. For that method first of all, 1M solutions of $Cl_2Ni.6H_2O$, $FeCl_3.6H_2O$ and $Ba(NO_3)_2$were prepared separately in DI water. A mixture was taken by adding 10mL from each solution and then 4N solution of NaOH was added dropwise with constant magnetic stirring until pH reached at 12 that ensured the complete precipitation of cations. Afterwards solution mixture was shifted to Teflon lined autoclave and reaction was carried out at 180ºC for 24h. After cooling of autoclave, the product was washed 3 times by centrifugation with distilled water and 1 time with ethanol @ 8000rpm for 10min in each case. Finally, the sample was dried in vacuum oven at 100°C for 24h. In order to obtain finely divided powder the product was ground in pestle and mortar [83]. For barium doped nickel ferrite nanoparticles synthesis different molar volume solutions of barium chloride and nickel chloride were prepared by dissolving stoichiometric amount of barium nitrate and nickel chloride respectively in DI water. These solutions were then added in 1M solutions of ferric chloride followed by similar procedure [84]. Figure 3.1 shows the flow chart for synthesis of Ba doped Ni ferrite nanoparticles:

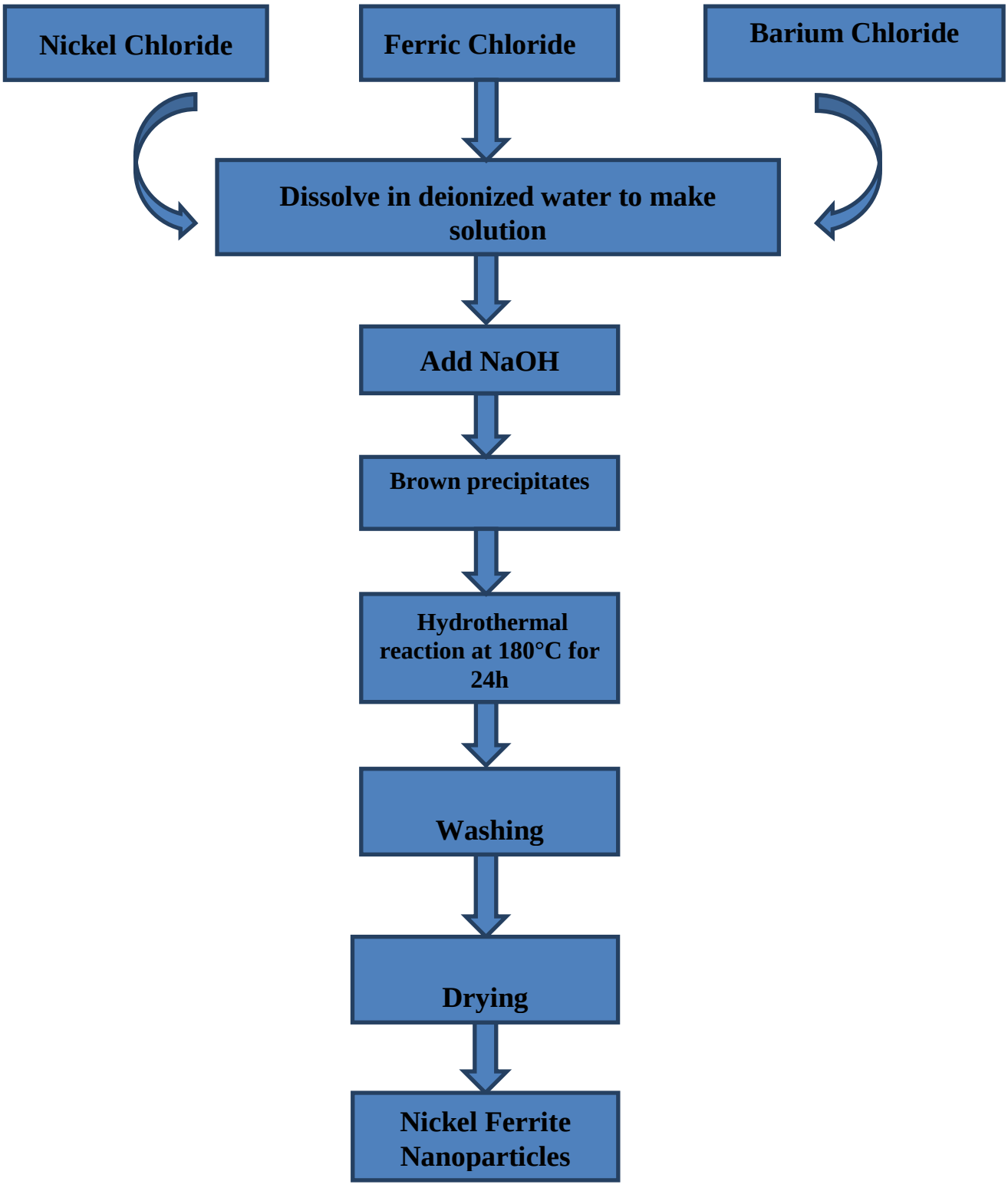

Figure 3.1: Flow chart for synthesis of Ba doped Ni-Ferrite nanoparticles.

3.2. Characterization.

The crystal structure of synthesized samples in solid and annealed states were analyzed in $80°<2\theta<100°$ range by X-Ray powder diffraction (D8 ADVANCE) device having Cuk_{α} (λ = 1.5418 Å) monochromatic radiation and operating at 40kV. Then POWDER CELL program was used for qualitative analysis [85] while in order to perform quantitative analysis Rietveld refinements was done by FULLPROF program [86].

To verify sample morphologies, qualitative analysis and shape hierarchy, scanning electron microscopy (SEM) was performed through Electron Probe Micro analysis (EPMA) on MIRA3 TESCAN Zeiss Supra 55VP coupled with EDX having magnification power 25kx and working at 10kV over the powder samples coated with Au.

3.3. UV-Vis Spectroscopy.

Optical properties were done by UV/VIS spectrophotometer (Perkin Elmer) having spectral range 190-3300cm^{-1} over the sample suspension in DI water. Results were obtained in form of spectrum that were further used to calculate band gap.

3.4. LCR Meter.

The pellets of dia=12mm and thickness=2.3mm were mechanically prepared by means of hydraulic press using 10Mpa pressure at room temperature. Then for measurement of dielectric properties at room temperature pellets were placed one by one between the electrodes of LCR meter [Wayne Kerr version 6500B] having frequency ranging 100Hz-5MHz.

In order to measure magnetic properties Fluxgate Magnetometer was used.

Chapter 4

Results and Discussion

This chapter comprises of results and discussion of synthesis, characterization and physical properties of nanoferrites under consideration.

4.1. Characterization Techniques.

In order to characterize the samples different characterization techniques like XRPD, SEM and EDX were employed.

4.1.1. X-Ray Powder Diffraction. In order to determine phase, crystallite size and crystal structure XRPD has been used. The detailed analysis shows that Barium doped Nanoparticles have cubic crystal structure with $Fd\bar{3}m$ (227) space group that further confirm the formation of spinel cubic structure according to JCPDS Card No.10-325. The lattice parameters, cell volume and density obtained by generalized harmonic description via Rietveld refinement are shown in table 4.1.The number in brackets provides the deviation from least significant values of parameter [87].

Crystallite size was determined by using Debye-Scherrer formula [88]. The decrease in crystallite size and shifting of peaks towards lower angle can be described on the basis of larger ionic radii of dopant which causes internal stress. As nickel ferrites have inverse cubic spinel structure in which nickel ions are present at octahedral sites while Ba ions must preferentially be present at tetrahedral sites and it can be confirmed by increase in intensity of (220), (440) and (511) reflection planes that are more sensitive to ions present at tetrahedral and octahedral sites [89]. The impurity peaks (*) is present in $NiFe_2O_4$ sample which refers to iron oxide PDF, [Card No. 00-024-0081] with increase in dopant concentration intensity of impurity peak decreases and finally disappear after x=0.2, T.Vigneswari also observed same impurity peaks in calcium doped nickel ferrite nanoparticles synthesized by coprecipitation method [90] while impurity (+) refers to $BaFe_2O_4$ PDF, [Card No. 00-046-0113] and its intensity increases with increasing Ba concentration.

Table 4.1. Lattice parameters & density of prepared samples

Sample Type	Lattice Parameters(Å)	Density(g/cm^3)	Ref.
$NiFe_2O_4$	a=b=c=8.3499(1)	5.596	[This work]
$Ba_{0.2}Ni_{0.8}Fe_2O_4$	a=b=c=8.320(2)	4.365	[This work]

$Ba_{0.4}Ni_{0.6}Fe_2O_4$	a=b=c=8.345(2)	5.157	[This work]
$Ba_{0.6}Ni_{0.4}Fe_2O_4$	a=b=c=8.337(3)	5.205	[This work]
$Ba_{0.8}Ni_{0.2}Fe_2O_4$	A=8.45, b=19.04, c=5.38	5.345	[This work]
$BaFe_2O_4$	a=8.441(1), b=18.556(2), c=5.450(3)	3.629	[This work]

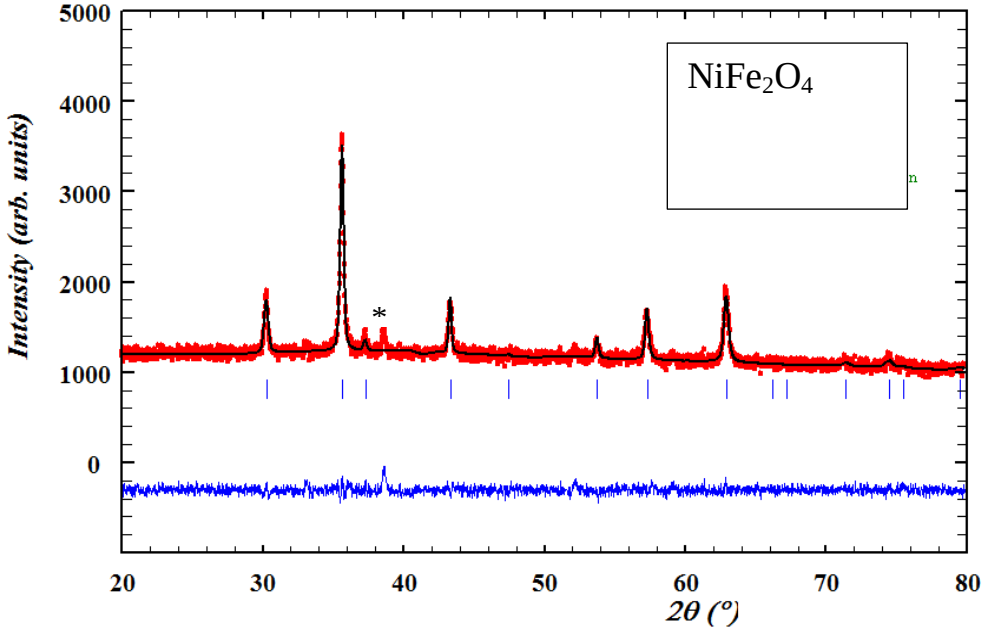

Figure 4.1 Refined XRD pattern of $NiFe_2O_4$

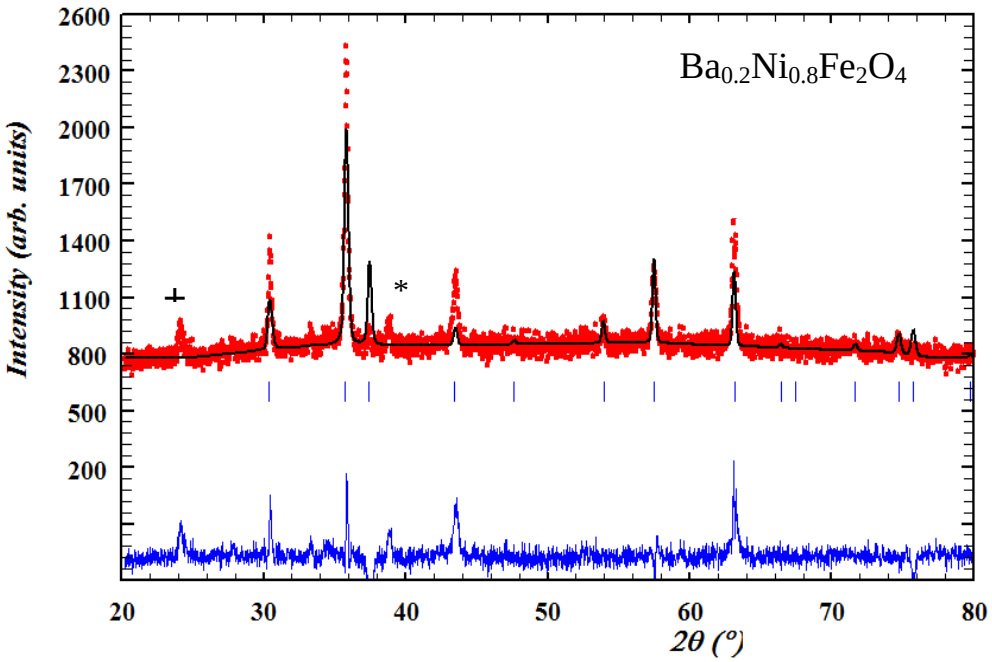

Figure 4.2. Refined XRD pattern of $Ba_{0.2}Ni_{0.8}Fe_2O_4$

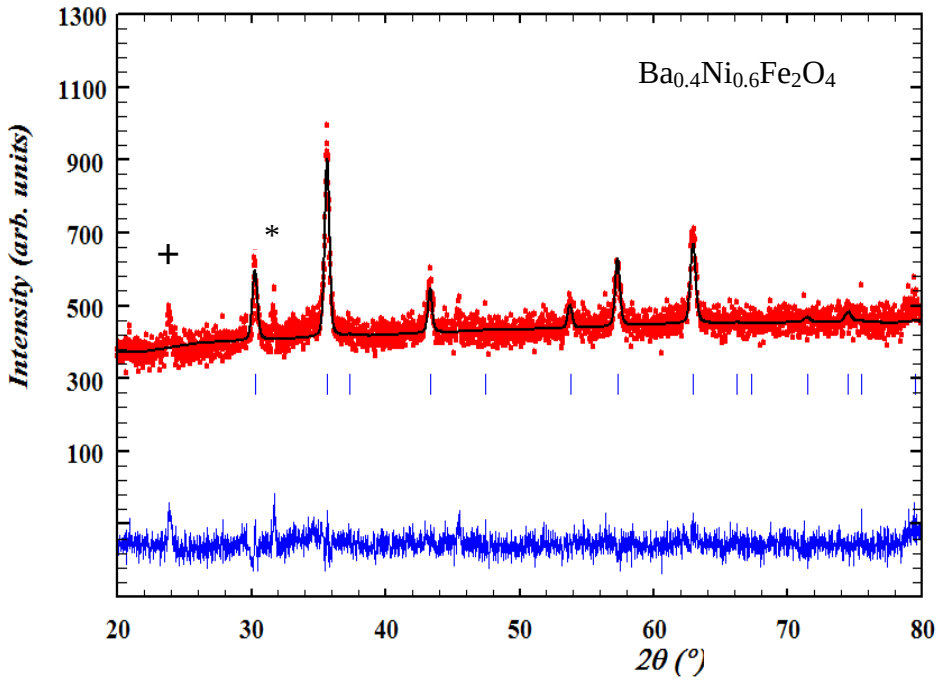

Figure 4.3. Refined XRD pattern of $Ba_{0.4}Ni_{0.6}Fe_2O_4$

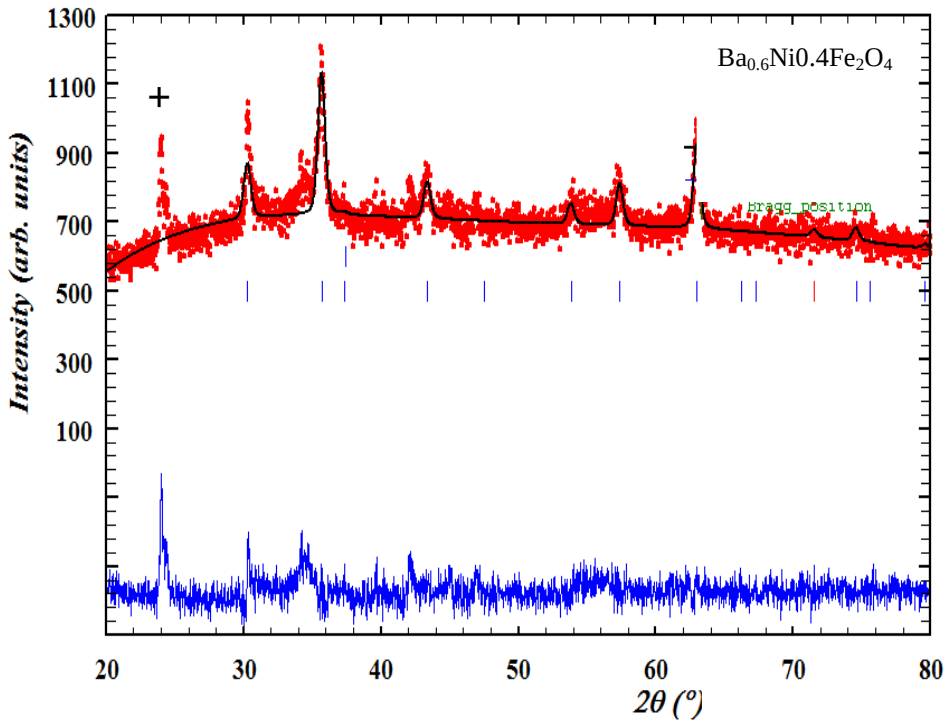

Figure 4.4. Refined XRD Pattern of $Ba_{0.6}Ni_{0.4}Fe_2O_4$

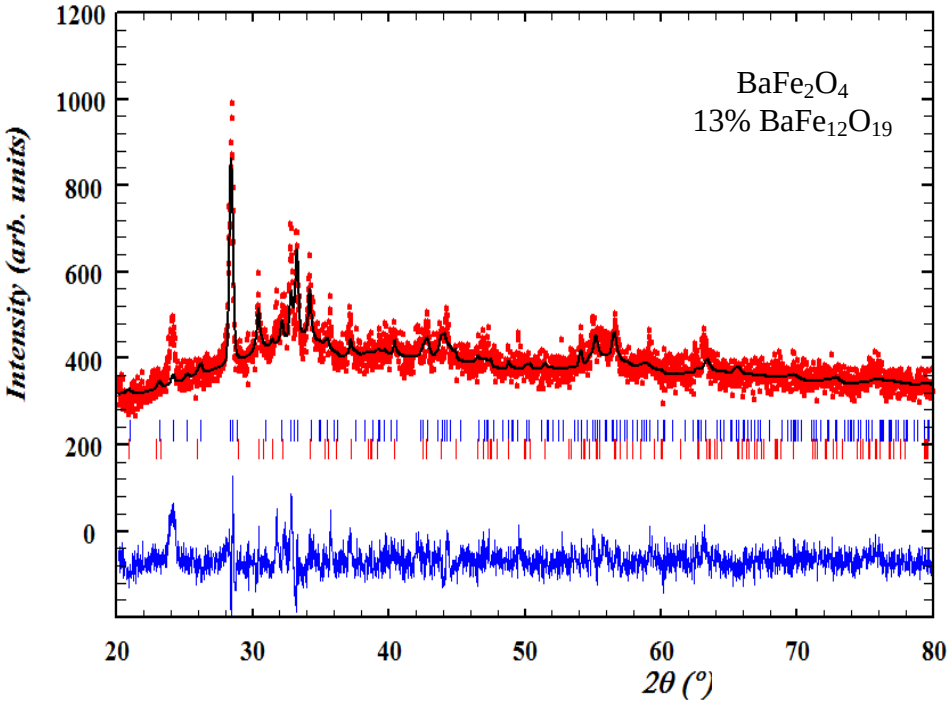

Figure 4.5. Refined XRD Pattern of $BaFe_2O_4$

Table 4.2. Crystallite size obtained from Debye-Scherrer equation and strain for prepared Samples

Sample Name	Crystallite size(nm)	Strain ($1/D^2$)	Ref.
$NiFe_2O_4$	71.6	19.5×10^{-5}	[This work]
$Ba_{0.2}Ni_{0.8}Fe_2O_4$	62.4	25.68×10^{-5}	[This work]
$Ba_{0.4}Ni_{0.6}Fe_2O_4$	52	36.9×10^{-5}	[This work]
$Ba_{0.6}Ni_{0.4}Fe_2O_4$	48.6	42.3×10^{-5}	[This work]
$Ba_{0.8}Ni_{0.2}Fe_2O_4$	42.8	92.9×10^{-5}	[This work]
$BaFe_2O_4$	45.2	48.9×10^{-5}	[This work]

4.1.2. Scanning Electron Microscopy. SEM was used for qualitative analysis and morphology of the samples. Figure 4.6 demonstrates the SEM micrographs of nickel ferrites and barium doped nickel ferrite nanoparticles, confirming the spherical shape. Moreover, it also indicates the agglomeration between these particles that can be explained on the basis of interaction between magnetic nanoparticles [91]. The particle size obtained from SEM is listed in table 4.3 that indicates there is gradual increase in particle size with increasing Ba contents and it is possibly due to larger ionic radii of dopant.

Table 4.3. Particles size obtained from SEM analysis for Ba doped Ni-Ferrite Nanoparticles $Ba_xNi_{1-x}Fe_2O_4$(x=0-0.6)

Sample Name	Particles Size(nm)
$NiFe_2O_4$	48.71
$Ba_{0.2}Ni_{0.8}Fe_2O_4$	61.57
$Ba_{0.4}Ni_{0.6}Fe_2O_4$	63.22
$Ba_{0.6}Ni_{0.4}Fe_2O_4$	66.78

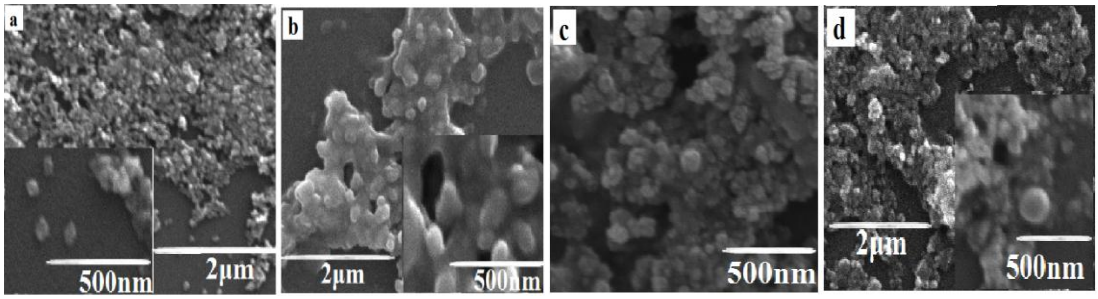

Figure 4.6. SEM images for prepared Nanoparticles a) $NiFe_2O_4$, b) $Ba_{0.2}Ni_{0.8}Fe_2O_4$, c) $Ba_{0.4}Ni_{0.6}Fe_2O_4$ and d) $Ba_{0.6}Ni_{0.4}Fe_2O_4$.

4.1.3. Energy Dispersive X-Ray Spectroscopy. EDX was used for the stoichiometry confirmation of prepared nanoparticles. Figure 4.7 shows the EDX pattern of sample while atomic percentage of elements present in sample are listed in table 4.4. The additional peaks in EDX patterns can be credited to gold coating and sample holder material. No impurity peak was observed in EDX spectra that revealed the purity of preprared samples.

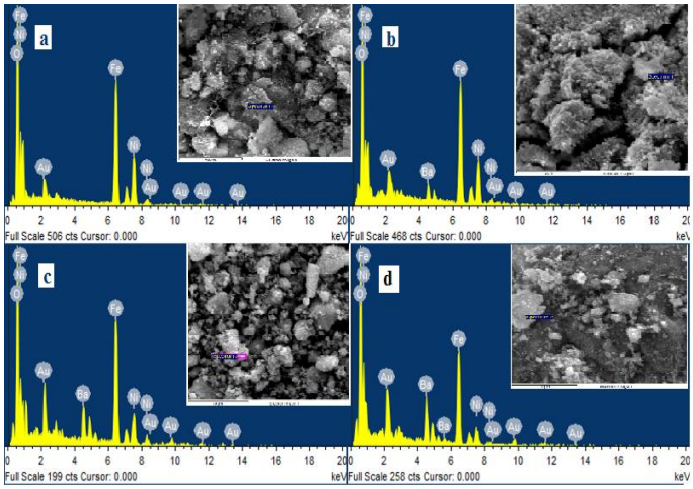

Figure 4.7. EDX Micrographs for prepared Nanoparticles a) $NiFe_2O_4$, b) $Ba_{0.2}Ni_{0.8}Fe_2O_4$, c) $Ba_{0.4}Ni_{0.6}Fe_2O_4$ and d) $Ba_{0.6}Ni_{0.4}Fe_2O_4$.

Table 4.4. Atomic percentage composition from EDX in Ba doped Ni-Ferrite Nanoparticles $Ba_xNi_{1-x}Fe_2O_4$(x=0-0.6)

Elements (at %)	$Ba_xNi_{1-x}Fe_2O_4$			
	x=0	x=0.2	x=0.4	x=0.6
O	76.07	75.95	75.74	80.52
Fe	15.05	15.03	16.08	13.16
Ni	8.88	7.80	5.32	2.91
Ba	-	1.22	2.86	3.40

4.2. Physical Properties.

Different physical properties like band gap, dielectric and magnetic properties has been determined by UV-Vis spectrophotometer, LCR meter and Flux Gate magnetometer respectively.

4.2.1 UV-Vis Spectroscopy. Absorbance spectrum was obtained with help of UV-Vis spectrophotometer. Barium dopant effect on optical band gap was analyzed by constructing Tauc Plot from absorbance spectrum. In Tauc Plot the optical band gap is analyzed by plotting graph between $(\alpha hv)^m$ (y-axis) and hv (x-axis) and then extrapolating tangent on x-axis. The change in values of absorption coefficient w.r.t hv (Photon energy) is specified as.

$$(\boldsymbol{ahv})^{\boldsymbol{m}} = \boldsymbol{A}(\boldsymbol{hv} - \boldsymbol{Eg})^{\boldsymbol{m}}$$

Where, α is absorption coefficient, hν is photon energy, A is edge width parameter, E_g is Band gap energy and m is 2 for direct band gap [92]. The values of optical band gap obtained for barium doped nickel Ferrite nanoparticles ranging from 5.2-5.5eV while 2.1ev and 5.7ev are band gap values of nickel ferrite and barium ferrite nanoparticles respectively as shown in Figure 4.9. These results show that optical band gap value is increased by increasing doping concentration. The phenomenon of increasing E_g values may be due to number of reasons like structural changes, decrease in crystallite size, change in lattice parameters and pressure induced effect etc. As by increasing doping concentration crystallite size is reduced leading to increase in band gap. Hence the values of band gap clearly reflect the theory of quantum size effect in doped nanoparticles [93].

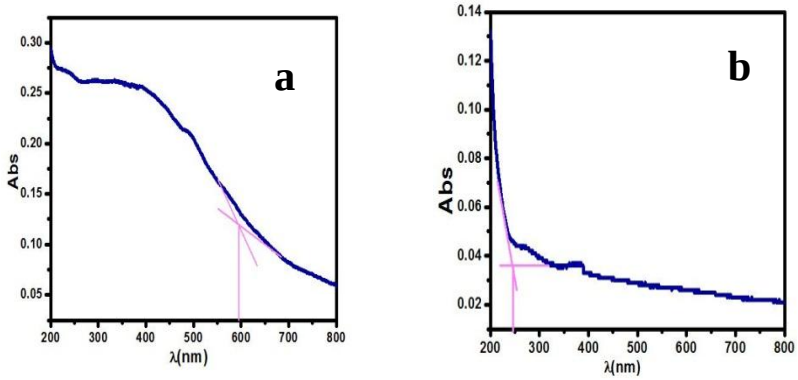

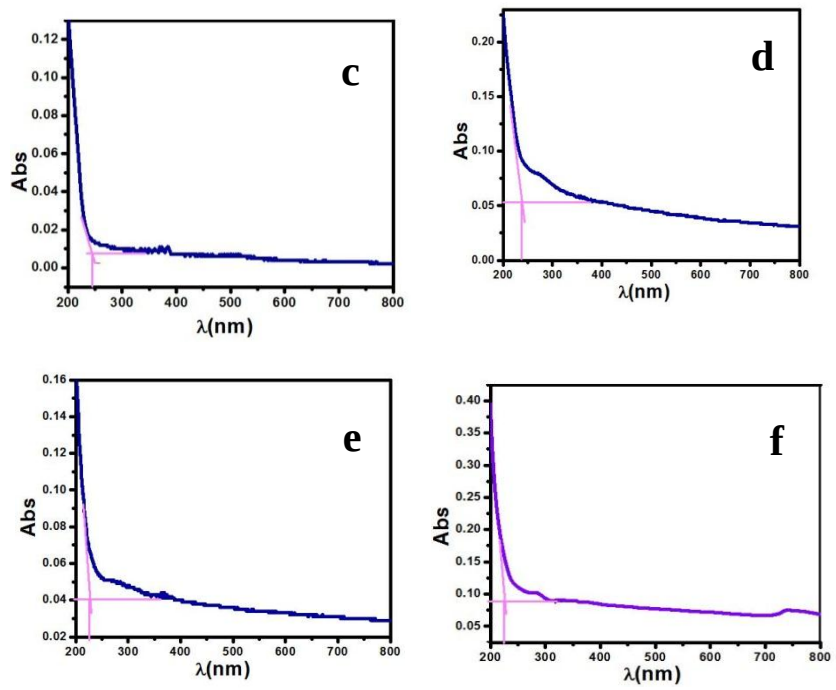

Figure 4.8. Absorbtion vs wavelength graphs of prepared samples a) $NiFe_2O_4$, b) $Ba_{0.2}Ni_{0.8}Fe_2O_4$, c) $Ba_{0.4}Ni_{0.6}Fe_2O$, d) $Ba_{0.6}Ni_{0.4}Fe_2O_4$, e) $Ba_{0.8}Ni_{0.2}Fe_2O_4$, f) $BaFe_2O_4$

Table 4.5. Band gap obtained by Tauc plot of prepared samples

Sample Name	Band gap (ev)
$NiFe_2O_4$	2.1
$Ba_{0.2}Ni_{0.8}Fe_2O_4$	5.2
$Ba_{0.4}Ni_{0.6}Fe_2O_4$	5.38
$Ba_{0.6}Ni_{0.4}Fe_2O_4$	5.45
$Ba_{0.8}Ni_{0.2}Fe_2O_4$	5.5
$BaFe_2O_4$	5.7

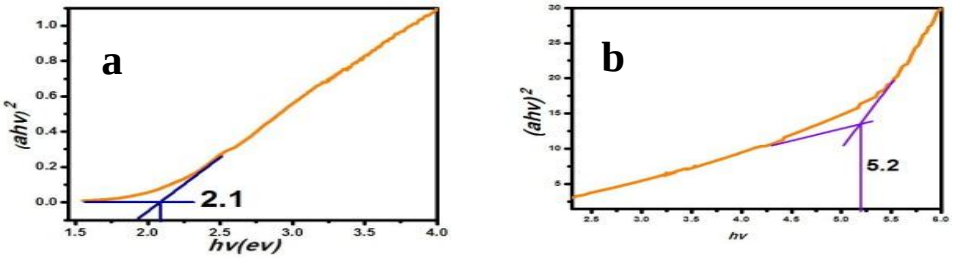

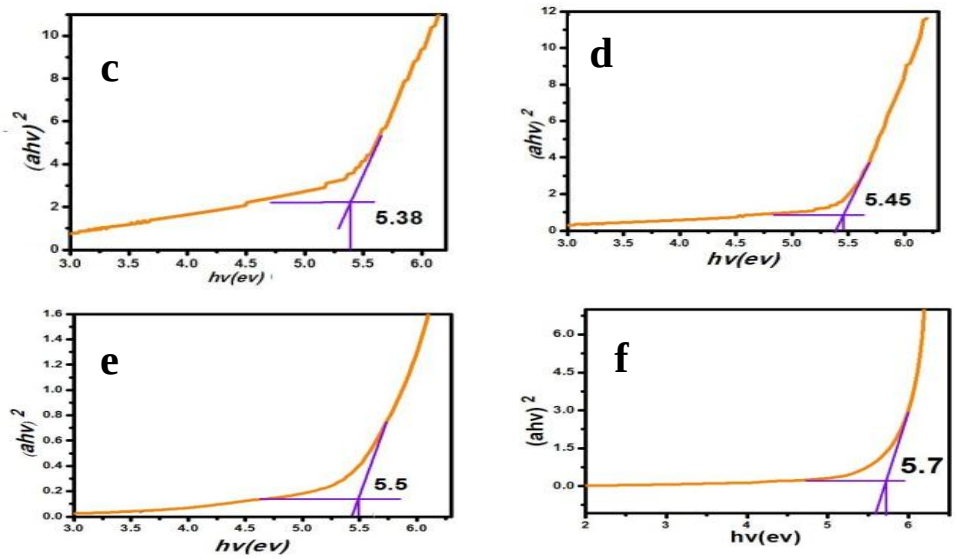

Figure 4.9. TaucPlot of prepared samples a) $NiFe_2O_4$, b) $Ba_{0.2}Ni_{0.8}Fe_2O_4$, c) $Ba_{0.4}Ni_{0.6}Fe_2O$, d) $Ba_{0.6}Ni_{0.4}Fe_2O_4$, e) $Ba_{0.8}Ni_{0.2}Fe_2O_4$, f) $BaFe_2O_4$

4.2.2. Dielectric Properties. By using the values of dissipation or D-Factor and parallel equivalent capacitance (Cp) that are obtained by the LCR meter at suitable range of frequency (*f*) different parameters like dielectric constant (ε′), dielectric loss (ε"), (tan δ) and AC conductivity have been investigated. These parameters give useful information about dielectric behavior of material, i.e. dielectric constant gives information about capability of material to store electric energy or in other words tell about polarizability of material.

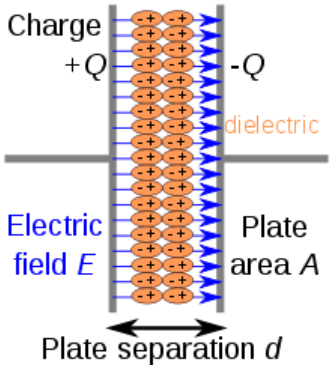

Figure 4.10. Schematic Diagram of Polarized Dielectric Material

Basically, it is the ratio of the material's permittivity to that of free space. Dielectric constant can be calculated by using given below expression.

$$\varepsilon' = \frac{CD}{\varepsilon^{\circ}A}$$

Here C is the capacitance, D is the thickness of pallet, A is surface area of sample and ε° is the Permittivity of free space (8.85×10^{-12} Fm^{-1}) [94]. Figure 4.11 shows that value of dielectric constant linearly decreases by increasing value of frequency that is normal behavior of spinal ferrites and have also been reported earlier [95] as well. This can be described by dipole relaxation phenomenon which is lag in the dielectric medium response to applied electric field. Generally ferrites have heterogeneous structure composed of appreciable conducting grains that are separated by almost non conducting grain boundaries [96]. Polarization is produced as a result of stacking up the electrons at grain boundaries due to high resistance at grain boundaries. But, at higher frequency mostly the electrons reverse their direction of motion causing decrease in the number of electrons at the grain boundary and as a result polarization decreases [97]. Moreover, at higher frequency the electron exchange $Fe^{2+}\rightarrow Fe^{3+}$ cannot follow the alternating electric field variations which led to decrease in dielectric constant. It was observed that sample with x=0.8 show maximum value of dielectric constant this is due to decrease in crystallite size that led to increase in number of nonconducting grain boundaries at specific area. The different values of dielectric constant for samples with different compositions are due to difference in presence of defects, porosity, metals ions (Fe^{2+}, Ni^{2+} and Ba^{2+}) and oxygen vacancies etc. [98].

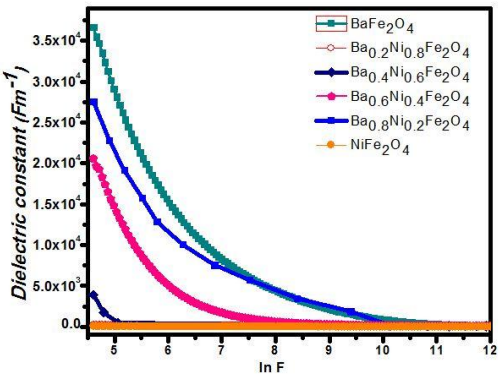

Figure 4.11. Dielectric Constant vs ln F plot for Ba doped Ni-Ferrite nanoparticles

$$Ba_xNi_{1-x}Fe_2O_4\,(0\leq x\geq 1)$$

The imaginary part to determine dissipation of electromagnetic energy during alignment of particles along electric field due to defects, porosity or dislocation is known as dielectric loss (ε") and is calculated as [99] mentioned below,

$$\boldsymbol{\varepsilon'' = \varepsilon' \times Dfactor}$$

As shown in figure 4.12 the samples with low concentration of barium have less dielectric loss values may be due to following reasons like samples have high density with low porosity and are structurally perfect [100]. But as the concentration of dopant increases dielectric loss going to increase because more dissipation of heat in order to transfer electrons from one atom to another. The decrease in dielectric loss with increasing frequency may be due decrease in consumption of energy for electrons hopping because atom show slow movement of electrons [101].

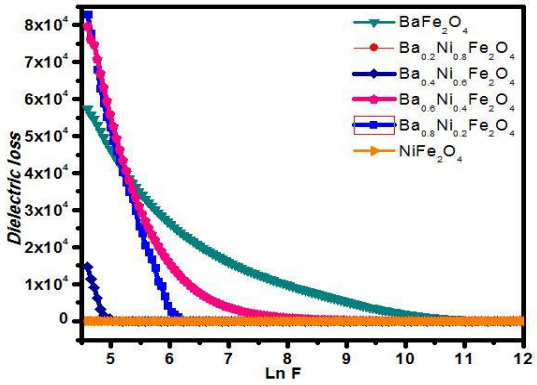

Figure 4.12. Dielectric loss vs ln F plot for Ba doped Ni-Ferrite nanoparticles

$$Ba_xNi_{1-x}Fe_2O_4\ (0\leq x\geq 1)$$

The real part for determination of dissipation or loss of energy is known as tangent loss (tan δ). Mathematically it can be expressed as follows [102].

$$\tan\delta = \frac{\varepsilon''}{\varepsilon'}$$

Graph shown in figure 4.13 for tan δ show a small decrease in the values of tangent loss at lower frequency because more time is offered for the movement of the electrons inside the grains at lower frequency. After that tangent loss start increasing as charge present in grains acts as a conductive medium so by increasing conduction the losses turned higher. Humps were observed as a result of Debye-type relaxation. This condition is created when the hopping frequency of ions becomes equal to applied field frequency. At last there is a sharp decrease in tangent loss values and then become constant .Decrease in values may be directly relate to decrease in conduction while constant behavior can be explained by absence of enough energy for polarization.

An increase in Ba concentration causes increase in tangent losses may be due to less Fe^{2+} →Fe^{3+} conversion. Since conduction is due to Fe^{2+} therefore increase in number of Fe^{2+} causes more energy losses [103].

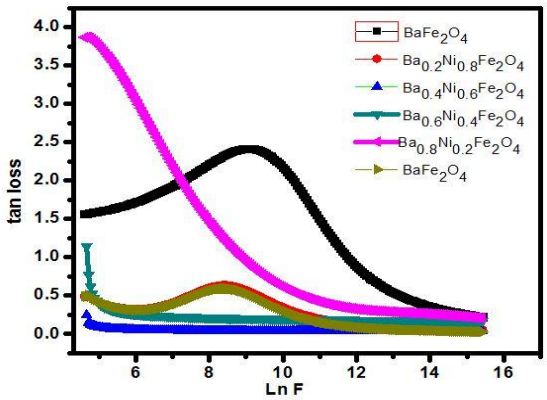

Figure 4.13. tan loss vs ln F graph for Ba doped Ni-Ferrite nanoparticles

$$Ba_xNi_{1-x}Fe_2O_4\ (0\leq x\geq 1)$$

AC conductivity can be defined as the capability of material to allow passage of alternating current and mathematically it can be expressed as [104].

$$\boldsymbol{\sigma_{ac} = 2\pi f \varepsilon^{\circ} \varepsilon''}$$

Graph in figure 4.14 shows that values of AC conductivity for all samples are almost constant at start but as the frequency increase AC conductivity also increases. This constant behavior of values can be described by Maxwell-Wagner model and Koop's theory.

According to these theories, Ferrites consists of two layers one is conducting layer comprising of conducting grains while other is poorly or nonconducting layer composed of nonconducting grain boundaries. Koop suggested that grain and grain boundary effect dominates at higher and lower frequencies, respectively. So at higher frequencies more AC conductivity due to dominating effect of conducting grains. But overall no periodic trend was observed in the values of AC conductivity. An increase in conductivity with increase in Ba concentration may be due to presence of more Fe^{3+} at octahedral sites causing less separation between Fe^{2+} and Fe^{3+} and as a result conduction increases due to increased hopping of charge carriers [105].

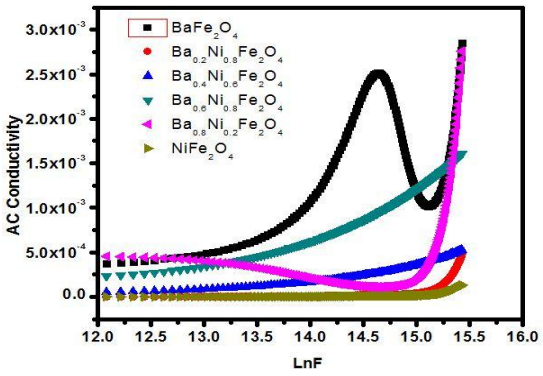

Figure 4.14. AC conductivity vs ln F plot for Ba doped Ni-Ferrite nanoparticles $Ba_xNi_{1-x}Fe_2O_4$ ($0 \leq x \geq 1$)

4.2.3. Magnetic Properties. The magnetic properties of all the samples were determined by Fluxgate DC magnetometer. Figure 4.15 represents the hysteresis loop of all samples observed at room temperature**.**

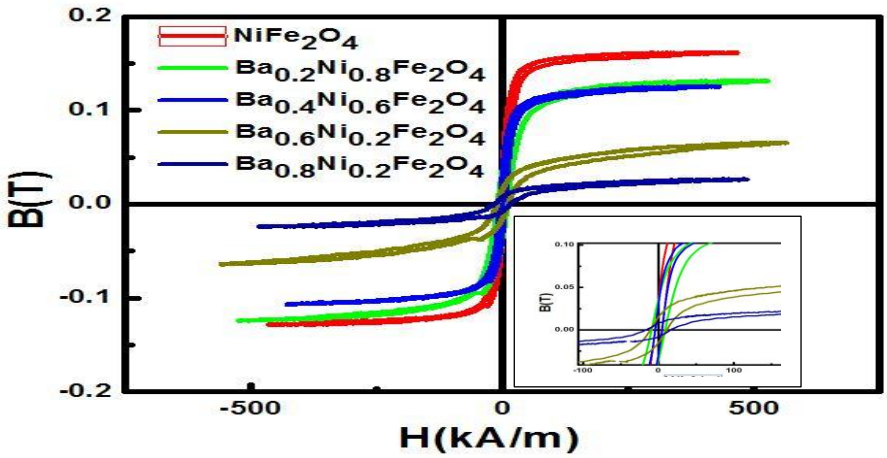

Figure 4.15. Hysteresis loop of samples observed at room temperature: inset shows the coercivity (Hc) of samples.

According to observed hysteresis loop of all samples it is noted that by increasing the concentration of barium value of saturation magnetization (Ms) decreases as shown in figure 4.16(a) and this can be explained on the basis of number of factors like decrease in crystallite size, redistribution of cations and surface spin disorder. Moreover, Barium is nonmagnetic and have zero magnetic moment and it can also leads to decrease in saturation magnetization. Generally, in spinel structures ferromagnetism is due to super exchange interactions between metal cations at octahedral (B) and tetrahedral (A) sites. As the barium concentration increases this causes the decrease in Fe ions at tetrahedral sites resulting strengthen of A-A and B-B interactions while weakening of A-B interactions [106]. Increase in barium

concentration leads to increase in coercivity values as shown in figure 4.16(b). This is due to fact that barium causes increase in magneto crystalline anisotropy and also it can be related to decrease in crystallite size as decrease in crystallite or grain size causes more number of grain boundaries hence more field is required for alignment of magnetic domains [107].

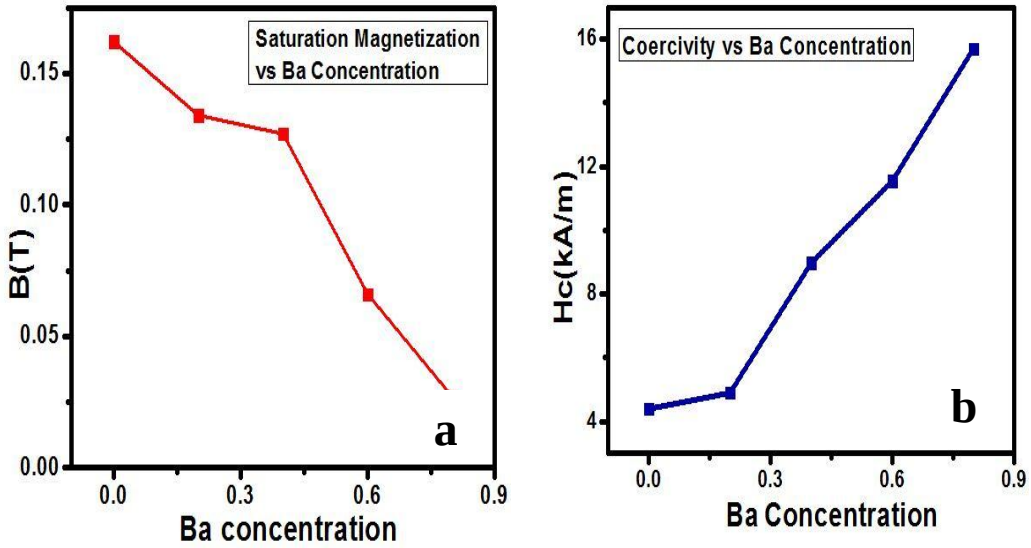

Figure 4.16. a) Graph of Ms vs Ba Concentration: b) Graph of Hc vs Ba concentration

Table 4.6. Values of Saturation magnetization and coercivity vs Barium concentration

Ba Concentration	Ms(T)	Hc(kA/m)
$NiFe_2O_4$	0.162	4.4
$Ba_{0.2}Ni_{0.8}Fe_2O_4$	0.134	4.9
$Ba_{0.4}Ni_{0.6}Fe_2O_4$	0.127	8.98
$Ba_{0.6}Ni_{0.4}Fe_2O_4$	0.066	11.55
$Ba_{0.8}Ni_{0.2}Fe_2O_4$	0.027	15.705

Conclusions and Future Prospects

In order to study the effect of barium doping in nickel ferrite nanoparticles on its optical, Dielectric and magnetic properties detailed study has been done. Barium doped nickel ferrites nanoparticles $Ba_xNi_{1-x}Fe_2O_4$ have been successfully synthesized and then characterized by XRD, SEM and EDX. XRD analysis confirmed the formation of cubic spinel structure. The crystallite size of prepared nanoparticles was calculated through Scherer's equation. The particles of samples have sperical in shape and were determined by SEM. EDX spectra revealed the purity of samples.

An increase in concentration of barium leads to increase in Band gap values from 2.1 to 5.2, 5.38, 5.45 and 5.5ev. Dielectric properties i.e dielectric constant, Dielectric loss, tan loss and AC were also studied which showed that these properties can easily controlled by varying particles size and barium concentration. Values of dielectric constant and dielectric loss have similar trend and both have highest values for maximum concentration of barium. Higher values of Dielectric constant are mainly due to interfacial and dipolar polarization. AC conductivity of all samples is almost constant at lower frequencies while they have maximum values at higher frequencies Hopping phenomenon was also observed in case of tan loss and AC conductivity. The investigation of magnetic properties revealed that increment of barium concentration causes reduction in values of saturation magnetization (Ms) from 0.162T to 0.027T and increase in coercivity (Hc) values from 4.4kA/m to 15.705kA/m. All these optical, dielectric and magnetic properties depend on crystallite size of samples.

Depending on observed optical, dielectric and magnetic properties the prepared samples can be used for energy storage, microwave absorption applications and in magnetic core devices.

1

References

1. National Nanotechnology Initiative. "FAQs: nanotechnology."*URL: http://www. nano. gov/nanotech-101/nanotechnology-facts (08.01. 14)* (2010).
2. Pokropivny, V. V., and V. V. Skorokhod. "Classification of nanostructures by dimensionality and concept of surface forms engineering in nanomaterial science." *Materials Science and Engineering: C* 27.5-8 (2007): 990-993.
3. Stone, V., Nowack, B., Baun, A., van den Brink, N., von der Kammer, F., Dusinska, M., and Fernandes, T. F. "Nanomaterials for environmental studies: classification, reference material issues, and strategies for physico-chemical characterisation." *Science of the total environment* 408.7 (2010): 1745-1754.
4. Pascu, S. I., Arrowsmith, R. L., Bayly, S. R., Brayshaw, S., and Hu, Z. "Towards nanomedicines: design protocols to assemble, visualize and test carbon nanotube probes for multi-modality biomedical imaging." *Philosophical Transactions of the Royal Society of London A: Mathematical, Physical and Engineering Sciences* 368.1924 (2010): 3683-3712.
5. Abdullaeva, Zhypargul. "Classification of Nanomaterials." *Nano-and Biomaterials: Compounds, Properties, Characterization, and Applications* (2017): 27-56.
6. Cao, Guozhong. *Nanostructures & nanomaterials: synthesis, properties & applications*. Imperial college press, 2004.
7. Sugimoto, Mitsuo. "The past, present, and future of ferrites." *Journal of the American Ceramic Society* 82.2 (1999): 269-280.
8. Hilpert, Siegfried, and Vom Verf. "Genetische und konstitutive Zusammenhänge in den magnetischen Eigenschaften bei Ferriten und Eisenoxyden." *Berichte der deutschen chemischen Gesellschaft* 42.2 (1909): 2248-2261.
9. Kato, Y., and T. Takei. "Characteristics of metallic oxide magnetic."*Journal of the Institute Eletronic Engineering of Japan* 53 (1933): 408-412.
10. Néel, Louis. "Théorie du traînage magnétique des ferromagnétiques en grains fins avec application aux terres cuites." *Ann. géophys.* 5 (1949): 99-136.
11. Raghunathan, A., Melikhov, Y., Snyder, J. E., and Jiles, D. C. "Generalized form of anhysteretic magnetization function for Jiles–Atherton theory of hysteresis." *Applied Physics Letters* 95.17 (2009): 172510.
12. Snelling, E. C. "Soft Ferrites, Properties and applications, Butter worth and Co." *Ltd., London* (1988).

13. Mathew, Daliya S., and Ruey-Shin Juang. "An overview of the structure and magnetism of spinel ferrite nanoparticles and their synthesis in microemulsions." *Chemical Engineering Journal* 129.1-3 (2007): 51-65.
14. Srivastava, Richa, and B. C. Yadav. "Ferrite materials: introduction, synthesis techniques, and applications as sensors." *International Journal of Green Nanotechnology* 4.2 (2012): 141-154.
15. Venkatasubramanian, R., R. S. Srivastava, and R. D. K. Misra. "Comparative study of antimicrobial and photocatalytic activity in titania encapsulated composite nanoparticles with different dopants." *Materials Science and Technology* 24.5 (2008): 589-595.
16. Joshi, H. M., Lin, Y. P., Aslam, M., Prasad, P. V., Schultz-Sikma, E. A., Edelman, R., and Dravid, V. P. . "Effects of shape and size of cobalt ferrite nanostructures on their MRI contrast and thermal activation." *The Journal of Physical Chemistry C* 113.41 (2009): 17761-17767.
17. Wu, H., Liu, G., Wang, X., Zhang, J., Chen, Y., Shi, J., and Yang, S.. "Solvothermal synthesis of cobalt ferrite nanoparticles loaded on multiwalled carbon nanotubes for magnetic resonance imaging and drug delivery." *Acta biomaterialia* 7.9 (2011): 3496-3504.
18. Reddy, CV Gopal, S. V. Manorama, and V. J. Rao. "Preparation and characterization of ferrites as gas sensor materials." *Journal of materials science letters* 19.9 (2000): 775-778.
19. Lou, Jie-Chung, Yu-Jen Huang, and Jia-Yun Han. "Treatment of printed circuit board industrial wastewater by Ferrite process combined with Fenton method." *Journal of hazardous materials* 170.2-3 (2009): 620-626.
20. Kefeni, Kebede K., Titus AM Msagati, and Bhekie B. Mamba. "Ferrite nanoparticles: synthesis, characterisation and applications in electronic device." *Materials Science and Engineering: B* 215 (2017): 37-55.
21. Valenzuela, Raul. *Magnetic ceramics*. Vol. 4. Cambridge University Press, 2005.
22. Galvão, W. S., Neto, D., Freire, R. M., and Fechine, P. B. A. "Super-paramagnetic nanoparticles with spinel structure: a review of synthesis and biomedical applications." *Solid State Phenomena*. Vol. 241. Trans Tech Publications, 2016.
23. Galvão, W. S., Neto, D., Freire, R. M., and Fechine, P. B. A. "Super-paramagnetic nanoparticles with spinel structure: a review of synthesis and biomedical applications." *Solid State Phenomena*. Vol. 241. Trans Tech Publications, 2016.

24. Heck, Carl. *Magnetic materials and their applications*. Elsevier, 2013.
25. Tuller, Harry L. "Ionic conduction in nanocrystalline materials." *Solid State Ionics* 131.1-2 (2000): 143-157
26. Cheong, Sang-Wook, and Maxim Mostovoy. "Multiferroics: a magnetic twist for ferroelectricity." *Nature materials* 6.1 (2007):
27. Guo, J., Bamber, T., Chamberlain, M., Justham, L., and Jackson, M. "Optimization and experimental verification of coplanar interdigital electroadhesives." *Journal of Physics D: Applied Physics* 49.41 (2016): 415304.
28. Morrish, Allan H. "The physical principles of magnetism." *The Physical Principles of Magnetism, by Allan H. Morrish, pp. 696. ISBN 0-7803-6029-X. Wiley-VCH, January 2001*. (2001): 696.
29. O'handley, Robert C. *Modern magnetic materials: principles and applications*. Wiley, 2000.
30. Gupta, Nitish. "Current Development in Synthesis and Characterization of Nickel Ferrite Nanoparticle." *Materials Today: Proceedings* 4.2 (2017): 342-349.
31. Vigneswari, T., and P. Raji. "Structural and magnetic properties of calcium doped nickel ferrite nanoparticles by co-precipitation method." *Journal of Molecular Structure* 1127 (2017): 515-521.
32. Eckert, Michael. "Max von Laue and the discovery of X-ray diffraction in 1912." *Annalen der Physik* 524.5 (2012)
33. Cook, E., Fong, R., Horrocks, J., Wilkinson, D., and Speller, R. "Energy dispersive X-ray diffraction as a means to identify illicit materials: A preliminary optimisation study." *Applied Radiation and Isotopes* 65.8 (2007): 959-967.
34. Das, Rasel, Eaqub Ali, and Sharifah Bee Abd Hamid. "CURRENT APPLICATIONS OF X-RAY POWDER DIFFRACTION-A REVIEW."*Reviews on Advanced Materials Science* 38.2 (2014).
35. Ramachandran, Vangipuram Seshachar, and James J. Beaudoin. *Handbook of analytical techniques in concrete science and technology: principles, techniques and applications*. Elsevier, 2000.
36. Lou, B., Peng, B., Rong, N., Li, Y., Chen, H., Sree, K. S., and Varma, A. "Root and root endophytes from the eyes of an electron microscopist." *Root Engineering*. Springer Berlin Heidelberg, 2014. 469-486
37. Stokes, Debbie.*Principles and practice of variable pressure: environmental scanning electron microscopy (VP-ESEM)*. John Wiley & Sons, 2008.

38. Gotze, J., and U. Kempe. "A comparison of optical microscope-and scanning electron microscope-based cathodoluminescence (CL) imaging and spectroscopy applied to geosciences." *Mineralogical Magazine* 72.4 (2008): 909-924.
39. Lyman, C. E., Newbury, D. E., Goldstein, J., Williams, D. B., Romig Jr, A. D., Armstrong, J., and Peters, K. R.*Scanning electron microscopy, X-ray microanalysis, and analytical electron microscopy: a laboratory workbook*. Springer Science & Business Media, 2012.
40. Reimer, Ludwig. *Scanning electron microscopy: physics of image formation and microanalysis*. Vol. 45. Springer, 2013.
41. Goldstein, G. I.; Newbury, D. E.; Echlin, P.; Joy, D. C.; Fiori, C.; Lifshin, E. "*Scanning electron microscopy and x-ray microanalysis"*. New York: Plenum Press,(1981).
42. Suzuki, E. "High-resolution scanning electron microscopy of immunogold-labelled cells by the use of thin plasma coating of osmium". *Journal of Microscopy*, 2002 .208 (3): 153–157.
43. Langer, P., et al. "7A11-Laser induced emission of electrons, ions, and X rays from solid targets." *IEEE Journal of Quantum Electronics* 2.9 (1966): 499-506.
44. Lyman, C. E., Newbury, D. E., Goldstein, J., Williams, D. B., Romig Jr, A. D., Armstrong, J., and Peters, K. R.*Scanning electron microscopy, X-ray microanalysis, and analytical electron microscopy: a laboratory workbook*. Springer Science & Business Media, 2012.
45. Maenhaut, W., and H. Raemdonck. "Accurate calibration of a Si (Li) detector for PIXE analysis." *Nuclear Instruments and Methods in Physics Research Section B: Beam Interactions with Materials and Atoms* 1.1 (1984): 123-136.
46. Mo, L., Yang, L., Lee, E. H., and He, S. "High-efficiency plasmonic metamaterial selective emitter based on an optimized spherical core-shell nanostructure for planar solar thermophotovoltaics." *Plasmonics* 10.3 (2015): 529-538.
47. Rajput, R. K. *Elect & Electronic Measurement & Instrument*. S. Chand Limited, 2009.
48. Bakshi, U. A., and A. V. Bakshi. *Electronic Measurement Systems*. Technical Publications, 2009.
49. Primdahl, Fritz. "The fluxgate magnetometer." *Journal of Physics E: Scientific Instruments* 12.4 (1979): 241.

50. Geyger, William A. "New Type of Flux-Gate Magnetometer." *Journal of Applied Physics* 33.3 (1962): 1280-1281.
51. Hill, Roderick J., James R. Craig, and G. V. Gibbs. "Systematics of the spinel structure type." *Physics and chemistry of minerals* 4.4 (1979): 317-339.
52. Harris, Vincent G. "Modern microwave ferrites." *IEEE Transactions on Magnetics* 48.3 (2012): 1075-1104.
53. Bragg, W. H. "The structure of magnetite and the spinels." *Nature* 95.2386 (1915): 561
54. Galvão, W. S., Neto, D., Freire, R. M., & Fechine, P. B. A. "Super-paramagnetic nanoparticles with spinel structure: a review of synthesis and biomedical applications." *Solid State Phenomena*. Vol. 241. Trans Tech Publications, 2016
55. Chen, Dong-Hwang, and Xin-Rong He. "Synthesis of nickel ferrite nanoparticles by sol-gel method." *Materials Research Bulletin* 36.7-8 (2001): 1369-1377.
56. Atif, M., S. K. Hasanain, and M. Nadeem. "Magnetization of sol–gel prepared zinc ferrite nanoparticles: effects of inversion and particle size." *Solid state communications* 138.8 (2006): 416-421.
57. Maensiri, S., Masingboon, C., Boonchom, B., and Seraphin, S. "A simple route to synthesize nickel ferrite (NiFe2O4) nanoparticles using egg white." *Scripta Materialia* 56.9 (2007): 797-800.
58. Maaz, K., Karim, S., Mumtaz, A., Hasanain, S. K., Liu, J.,and Duan, J. L."Synthesis and magnetic characterization of nickel ferrite nanoparticles prepared by co-precipitation route." *Journal of Magnetism and Magnetic Materials* 321.12 (2009): 1838-1842
59. Wang, J., Ren, F., Yi, R., Yan, A., Qiu, G., and Liu, X ."Solvothermal synthesis and magnetic properties of size-controlled nickel ferrite nanoparticles."*Journal of Alloys and Compounds* 479.1-2 (2009): 791-796.
60. Rezlescu, N., Rezlescu, E., Doroftei, C., Popa, P. D., and Ignat, M."Semiconducting spinel ferrite powders prepared by self-combustion method for catalyst applications."*Semiconductor Conference (CAS), 2012 International*. Vol. 2. IEEE, 2012.
61. Singh, S., Yadav, B. C., Gupta, V. D., and Dwivedi, P. K. "Investigation on effects of surface morphologies on response of LPG sensor based on nanostructured copper ferrite system." *Materials Research Bulletin* 47.11 (2012): 3538-3547.

62. Nejati, Kamellia, and Rezvanh Zabihi. "Preparation and magnetic properties of nano size nickel ferrite particles using hydrothermal method."*Chemistry Central Journal* 6.1 (2012): 23.
63. Goswami, P. P., Choudhury, H. A., Chakma, S., and Moholkar, V. S. "Sonochemical synthesis of cobalt ferrite nanoparticles." *International Journal of Chemical Engineering* 2013 (2013)
64. Widatallah, H. M., Johnson, C., Berry, F., and Pekala, M. "Synthesis, structural, and magnetic characterisation of magnesium-doped lithium ferrite of composition Li0. 5Fe2. 5O4." *Solid state communications*120.4 (2001): 171-175.
65. Sattar, A. A., H. M. El-Sayed, and W. R. Agami. "Physical and magnetic properties of calcium-substituted Li-Zn ferrite." *Journal of Materials Engineering and Performance*16.5 (2007): 573-577.
66. . Bhushan, B., Basumallick, A., Bandopadhyay, S. K., Vasanthacharya, N. Y., and Das, D."Effect of alkaline earth metal doping on thermal, optical, magnetic and dielectric properties of BiFeO3 nanoparticles." *Journal of Physics D: Applied Physics* 42.6 (2009): 065004.
67. Shobana, M. K. "Calcium doped nickel ferrite powders prepared by sol-gel combustion method." *International Journal of Nano Dimension* 2.4 (2012): 275.
68. Bhushan, B. "Enhancing the magnetic characteristics of BiFeO3 nanoparticles by Ca, Ba co-doping."*Materials Chemistry and Physics* 135.1 (2012): 144-149.
69. Andoulsi, Refka, Karima Horchani-Naifer, and Mokhtar Férid. "Structural and electrical properties of calcium substituted lanthanum ferrite powders." *Powder technology* 230 (2012): 183-187.
70. Manikandan, A., Vijaya, J. J., Sundararajan, M., Meganathan, C., Kennedy, L. J., and Bououdina, M. "Optical and magnetic properties of Mg-doped ZnFe2O4 nanoparticles prepared by rapid microwave combustion method."*Superlattices and Microstructures* 64 (2013): 118-131.
71. . Chauhan, S., Arora, M., Sati, P. C., Chhoker, S., Katyal, S. C., & Kumar, M. "Structural, vibrational, optical, magnetic and dielectric properties of Bi1−xBaxFeO3 nanoparticles." *Ceramics International* 39.6 (2013): 6399-6405.
72. Gherca, D., et al. "Eco-environmental synthesis and characterization of nanophase powders of Co, Mg, Mn and Ni ferrites."*Ceramics International* 40.7 (2014): 9599-9607.

73. Chaudhuri, A., and K. Mandal. "Study of structural, ferromagnetic and ferroelectric properties of nanostructured barium doped Bismuth Ferrite." *Journal of Magnetism and Magnetic Materials* 353 (2014): 57-64.
74. Bamzai, K. K., et al. "Preparation, and Structural and Magnetic Properties of Ca Substituted Magnesium Ferrite with Composition MgCaxFe2− xO4 (= 0.00, 0.01, 0.03, 0.05, 0.07)." *Journal of Materials* 2014 (2014).
75. Dhir, Gitanjali, Poonam Uniyal, and N. K. Verma. "Effect of particle size on multiferroism of barium-doped bismuth ferrite nanoparticles." *Materials Science in Semiconductor Processing* 27 (2014): 611-618.
76. Nadeem, K., S. Rahman, and M. Mumtaz. "Effect of annealing on properties of Mg doped Zn-ferrite nanoparticles." *Progress in Natural Science: Materials International* 25.2 (2015): 111-116.
77. Moradmard, H., Shayesteh, S. F., Tohidi, P., Abbas, Z., and Khaleghi, M. "Structural, magnetic and dielectric properties of magnesium doped nickel ferrite nanoparticles."*Journal of Alloys and Compounds* 650 (2015): 116-122.
78. Srinivas, V., A. T. Raghavender, and K. Vijaya Kumar. "Effect of Ba Substitution on the Structural and Magnetic Properties of BiFeO3." *World Journal of Nano Science and Engineering*6.01 (2016): 38.
79. Sendhilnathan, S. "Enhancement in dielectric and magnetic properties of Mg^{2+} substituted highly porous super paramagnetic nickel ferrite nanoparticles with Williamson-Hall plots mechanistic view."*Ceramics International* 43.17 (2017): 15447-15453.
80. Mund, H. S., and B. L. Ahuja. "Structural and magnetic properties of Mg doped cobalt ferrite nano particles prepared by sol-gel method."*Materials Research Bulletin* 85 (2017): 228-233.
81. Vigneswari, T., and P. Raji. "Structural and magnetic properties of calcium doped nickel ferrite nanoparticles by co-precipitation method."*Journal of Molecular Structure* 1127 (2017): 515-521.
82. Chavan, Pradeep, and L. R. Naik. "Investigation of energy band gap and conduction mechanism of magnesium substituted nickel ferrite nanoparticles." *physica status solidi (a)* 214.9 (2017).
83. Vigneswari, T., and P. Raji. "Structural and magnetic properties of calcium doped nickel ferrite nanoparticles by co-precipitation method." *Journal of Molecular Structure* 1127 (2017): 515-521.

84. He, Hai-Yan. "Structural and Magnetic Property of Co1-xNixFe2O4 Nanoparticles Synthesized by Hydrothermal Method." *International Journal of Applied Ceramic Technology*11.4 (2014): 626-636.
85. Kraus, Werner, and Gert Nolze. "POWDER CELL–a program for the representation and manipulation of crystal structures and calculation of the resulting X-ray powder patterns." *Journal of Applied Crystallography* 29.3 (1996): 301-303.
86. Roisnel, T., and J. Rodriguez-Carvajal. "WinPLOTR: a Windows tool for powder diffraction analysis." *In Materials Science Forum. Proceedings of the European Powder Diffraction Conf.(EPDIC 7*. 2001.
87. Sivakumar, P., Ramesh, R., Ramanand, A., Ponnusamy, S., and Muthamizhchelvan, C."Synthesis and characterization of nickel ferrite magnetic nanoparticles." *Materials Research Bulletin*46.12 (2011): 2208-2211.
88. Holzwarth, Uwe, and Neil Gibson. "The Scherrer equation versus the'Debye-Scherrer equation'." *Nature nanotechnology* 6.9 (2011): 534.
89. Moradmard, H., Shayesteh, S. F., Tohidi, P., Abbas, Z., and Khaleghi, M.. "Structural, magnetic and dielectric properties of magnesium doped nickel ferrite nanoparticles." *Journal of Alloys and Compounds* 650 (2015): 116-122.
90. Vigneswari, T., and P. Raji. "Structural and magnetic properties of calcium doped nickel ferrite nanoparticles by co-precipitation method." *Journal of Molecular Structure* 1127 (2017): 515-521.
91. Moradmard, H., Shayesteh, S. F., Tohidi, P., Abbas, Z., and Khaleghi, M.. "Structural, magnetic and dielectric properties of magnesium doped nickel ferrite nanoparticles." *Journal of Alloys and Compounds* 650 (2015): 116-122.
92. Sivaraman, T., Narasimman, V., Nagarethinam, V. S., and Balu, A. R. "Effect of chlorine doping on the structural, morphological, optical and electrical properties of spray deposited CdS thin films." *Progress in Natural Science: Materials International* 25.5 (2015): 392-398
93. Yücel, Ersin, and Yasin Yücel. "Effect of doping concentration on the structural, morphological and optical properties of Ca-doped PbS thin films grown by CBD." *Optik-International Journal for Light and Electron Optics* 142 (2017): 82-89.
94. Sheng, Z. Z., and A. M. Hermann. "Superconductivity in the rare-earth-free TI—Ba—Cu—O system above liquid-nitrogen temperature." *Ten Years of Superconductivity: 1980–1990*. Springer, Dordrecht, 1993. 305-308.

95. Rafiq, U., Hanif, M., Anis-ur-Rehman, M., and ul Haq, A. "AC Electrical Properties of MgFe2− xNdxO4 (x= 0 to 0.04) for High Frequency Applications." *Journal of Superconductivity and Novel Magnetism* 30.12 (2017): 3559-3563.
96. Rani, R., Kumar, G., Batoo, K. M., and Singh, M. "Electric and dielectric study of zinc substituted cobalt nanoferrites prepared by solution combustion method." *American Journal of Nanomaterials* 1.1 (2013): 9-12.
97. Soibam, Ibetombi, N. Nilima, and S. Phanjoubam. "Dielectric studies of double sintered lithium zinc nickel ferrite prepared by citrate precursor method." *Am J Mater Sci Eng* 2 (2014): 24-27.
98. Reddy, M. P., Balakrishnaiah, G., Madhuri, W., Ramana, M. V., Reddy, N. R., Kumar, K. S., and Reddy, R. R. . "Structural, magnetic and electrical properties of NiCuZn ferrites prepared by microwave sintering method suitable for MLCI applications." *Journal of Physics and Chemistry of Solids* 71.9 (2010): 1373-1380.
99. El-Mallah, H. M. "AC electrical conductivity and dielectric properties of perovskite (Pb, Ca) TiO3 ceramic." *Acta Physica Polonica-Series A General Physics* 122.1 (2012): 174.
100. Rani, R., Kumar, G., Batoo, K. M., and Singh, M. "Electric and dielectric study of zinc substituted cobalt nanoferrites prepared by solution combustion method." *American Journal of Nanomaterials* 1.1 (2013): 9-12.
101. Rao, J. K., Raizada, A., Ganguly, D., Mankad, M. M., Satayanarayana, S. V., and Madhu, G. M. "Investigation of structural and electrical properties of novel CuO–PVA nanocomposite films." *Journal of materials science* 50.21 (2015): 7064-7074.
102. Noorkhan, Pathan Amjadkhan, and Sangshetty Kalayne. "Synthesis, Characterization Ac Conductivity Of Nickel Ferrite." *Journal of Engineering Research and Applications* 2 (2012): 681-685.
103. Rafiq, U., Hanif, M., Anis-ur-Rehman, M., and ul Haq, A. "AC Electrical Properties of MgFe2− xNdxO4 (x= 0 to 0.04) for High Frequency Applications." *Journal of Superconductivity and Novel Magnetism* 30.12 (2017): 3559-3563.
104. El-Mallah, H. M. "AC electrical conductivity and dielectric properties of perovskite (Pb, Ca) TiO3 ceramic." *Acta Physica Polonica-Series A General Physics* 122.1 (2012): 174.
105. Rafiq, U., Hanif, M., Anis-ur-Rehman, M., and ul Haq, A. "AC Electrical Properties of MgFe2− xNdxO4 (x= 0 to 0.04) for High Frequency

Applications."*Journal of Superconductivity and Novel Magnetism* 30.12 (2017): 3559-3563.

106. Moradmard, H., Shayesteh, S. F., Tohidi, P., Abbas, Z., and Khaleghi, M. "Structural, magnetic and dielectric properties of magnesium doped nickel ferrite nanoparticles."*Journal of Alloys and Compounds* 650 (2015): 116-122.

107. Anjana, V., John, S., Prakash, P., Nair, A. M., Nair, A. R., Sambhudevan, S., and Shankar, B. "Magnetic Properties of Copper Doped Nickel Ferrite Nanoparticles Synthesized by Co Precipitation Method." *IOP Conference Series: Materials Science and Engineering*. Vol. 310. No. 1. IOP Publishing, 2018.